

Primordial helium recombination. I. Feedback, line transfer, and continuum opacity

Eric R. Switzer*

Department of Physics, Princeton University, Princeton, New Jersey 08544, USA

Christopher M. Hirata

School of Natural Sciences, Institute for Advanced Study, Einstein Drive, Princeton, New Jersey 08540, USA

(Received 10 March 2007; published 30 April 2008)

Precision measurements of the cosmic microwave background temperature anisotropy on scales $\ell > 500$ will be available in the near future. Successful interpretation of these data is dependent on a detailed understanding of the damping tail and cosmological recombination of both hydrogen and helium. This paper and two companion papers are devoted to a precise calculation of helium recombination. We discuss several aspects of the standard recombination picture, and then include feedback, radiative transfer in He I lines with partial redistribution, and continuum opacity from H I photoionization. In agreement with past calculations, we find that He II recombination proceeds in Saha equilibrium, whereas He I recombination is delayed relative to Saha due to the low rates connecting excited states of He I to the ground state. However, we find that at $z < 2200$ the continuum absorption by the rapidly increasing H I population becomes effective at destroying photons in the He I $2^1P^o - 1^1S$ line, causing He I recombination to finish around $z \approx 1800$, much earlier than previously estimated.

DOI: [10.1103/PhysRevD.77.083006](https://doi.org/10.1103/PhysRevD.77.083006)

PACS numbers: 98.70.Vc, 95.30.Jx

I. INTRODUCTION

Cosmological recombination occurs when the photon gas in the early universe has cooled sufficiently for bound atoms to form. As the free electrons become locked in the ground states of these atoms, the opacity from Thomson scattering drops, and the signatures of thermal inhomogeneities in the recombination plasma begin to stream freely across the universe. These signatures reach us today in the cosmic microwave background (CMB). The best limits on the CMB temperature anisotropy over the sky, down to $\sim 0.4^\circ$ are provided by the Wilkinson Microwave Anisotropy Probe (WMAP) [1]. In conjunction with other surveys, these data tightly constrain cosmological model parameters [1,2].

Most future and recent CMB experimental efforts aim to measure the polarization or temperature anisotropy [3–16] on smaller scales than those measured by WMAP. Small-scale CMB temperature anisotropy measurements further constrain the matter and baryonic matter fractions, $\Omega_m h^2$ and $\Omega_b h^2$ [17], the spectral index of the primordial scalar power spectrum, n_s , and its possible running, α_s . Measurements of n_s will be integral to the viability or eventual rejection of a wide variety of inflation models [18,19].

The most conspicuous features in the CMB temperature anisotropy on small scales are acoustic oscillations [20–23] and Silk damping [24,25]. Silk damping is determined directly by the free electron abundance, which is set by the recombination history. Here, photons in the ionized gas will diffuse over a characteristic scale $k_D \propto \sqrt{n_e}$ (where n_e is the free electron number density and k_D is the damping

wave number), exponentially damping photon perturbations with wave numbers $k > k_D$. If the free electron density is overpredicted by recombination models, then k_D is also overpredicted and Boltzmann codes will predict too much power on small scales. Measurements of n_s using CMB data including the damping tail region will then be biased downward. In light of the WMAP 3-year analysis [1], it is crucial to understand how n_s differs from 1. While the differences among recently published recombination histories are too small to be important for the WMAP n_s measurement, the corrections are expected to be significant (at the $\Delta n_s \sim 0.02$ level) for Planck [26], and presumably also for high- ℓ experiments such as ACT [8] and SPT [9]. Successful interpretations of data from the next generation of small-scale CMB anisotropy experiments will depend on a solid understanding of recombination.

Fundamentally, the problem in cosmological recombination is to solve consistently for the evolution of the atomic level occupations and the radiation field (which has both a thermal piece, and a nonthermal piece from the radiation of the atoms themselves) in an expanding background. The highly excited states are kept close to equilibrium by the high rates interconnecting them, and the rate of formation of the ground state in both helium and hydrogen is dominated by the occupation of the $n = 2$ states and the rates connecting the $n = 2$ states to the ground state. In both helium and hydrogen, the decay channels to the ground state through the allowed transitions are dramatically suppressed relative to the vacuum rates by the optical depth in the gas. Indeed, in both systems, the two-photon decay rate from the $n = 2 S$ state (singlet in the case of He I) is comparable to the rate in allowed decay channels. This is the so-called “ $n = 2$ bottleneck” [27].

*switzer@princeton.edu

The primordial recombination was first investigated theoretically in the 1960s [28,29] using a simple “three-level atom” (TLA) approximation. The TLA tracks the abundance of ground state hydrogen atoms ($\text{H I } 1s$), excited hydrogen atoms (assumed to be in Boltzmann equilibrium), and free electrons. The TLA allows for recombination to and photoionization from excited H I levels, and allows excited atoms to decay to the ground state by $\text{Ly}\alpha$ ($2p \rightarrow 1s$) or two-photon ($2s \rightarrow 1s$) emission. Subsequently, a substantial literature developed, testing some of the assumptions of the TLA and extending it to the problem of helium recombination [30–35]. Seager *et al.* [27] provide the current benchmark precision recombination calculation by simulating 300 levels in H I , 200 levels in He I , 100 levels in He II , interactions with the radiation field in the Sobolev approximation, basic hydrogen chemistry, and matter temperature evolution. They found that the three-level model [28,29] with a “fudge factor” inserted to speed up H I recombination was an accurate approximation to their full multilevel atom solution. Their recombination code, RECFAST [36], is packaged into most of the CMB anisotropy codes in common use, and underlies the cosmological constraints from the CMB, including those recently reported by WMAP.

There are several reasons why it is now timely to revisit the cosmological recombination [37–39]. Recent work [40–51] has led to suspicion that some pieces of the recombination problem, such as matter temperature evolution [42,45], two-photon transitions from high-lying states [41,47,49], the effect of He I intercombination lines [41,43], departures of the l sublevels of hydrogen from their statistical population ratios [52], and stimulated two-photon transitions [40,44] are not completely understood or were absent in past work. Two-photon transitions and intercombination rates speed He I recombination by facilitating the formation of the ground state, and as described in [41] these could constitute a serious correction He I recombination, pushing He I much closer to equilibrium than in traditional models [27]. These considerations led to significant changes in cosmological model parameter estimates [26] and warrant further consideration. (The allowed, intercombination, quadrupole, and two-photon transitions up to $n = 3$ are shown in the Grotrian diagram, Fig. 1.) In addition, some of the issues considered during the 1990s, such as the effect of H I continuum opacity on He I recombination, were not fully resolved; we will show here that this problem is much more complicated than previously believed. Finally, the imminent prospect of precision CMB data at high ℓ from ACT, SPT, and Planck has “raised the bar” for theorists and demands a much better understanding of recombination than was needed a decade ago.

This is the first in a series of three papers devoted to the subject of helium recombination; the companion papers (C.M. Hirata and E.R. Switzer, following Article, Phys.

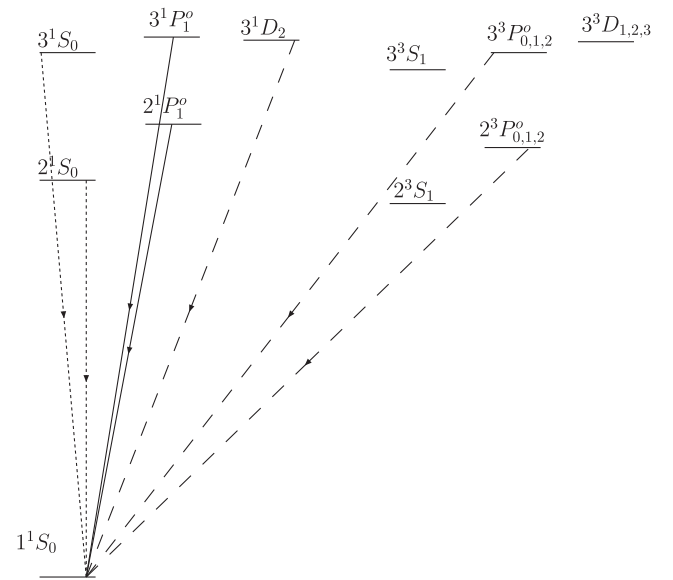


FIG. 1. Formation of neutral helium: a Grotrian diagram (up to $n = 3$) for He I . Singlet ($S = 0$ parahelium) and triplet ($S = 1$ orthohelium) levels and higher-order transitions give a rich system of low-lying transitions. Marked are two-photon transition (light dashed lines from 2^1S_0 and 3^1S_0), (allowed) electric dipole transitions (solid lines from $2^1P_1^o$ and $3^1P_1^o$, like the Lyman series in H I), the intercombination lines (heavy dashed lines from $2^3P_1^o$ and $3^3P_1^o$), and quadrupole transitions (from 3^1D_2). The dipole transitions are treated in Sec. VD using a Monte Carlo method with partial redistribution; forbidden one-photon lines are treated in Sec. IV using an analytic method for complete redistribution. (The energy levels are not drawn to scale.)

Rev. D **77**, 083007 (2008) and E.R. Switzer and C.M. Hirata, following Article, Phys. Rev. D **77**, 083008 (2008)) will be referred to as Paper II and Paper III. We have not yet completed the solution of hydrogen recombination because the radiative transfer is more complicated, the treatment of the high- n levels is more important, and the required accuracy is much greater. We do not believe our existing code is accurate enough for that application (see the discussion in Paper III). This paper describes the standard multilevel atom code, as well as the most important improvements we have made, namely, inclusion of feedback from spectral distortions, semiforbidden and forbidden lines, H I bound-free opacity, and radiative transfer in the He I lines in the cases of both complete and partial redistribution. Paper II describes several effects that we find to have only a small influence on recombination: two-photon transitions in He I , interfering damping wings, and photons in the He I continuum. Paper III discusses the effect of the isotope shift between ^3He and ^4He resonance lines, Thomson scattering, rare processes, collisional process, and peculiar velocities. Although we find these effects to be small, it is necessary to investigate them in order to be sure of this. Paper III also contains a summary of the

remaining uncertainty in helium recombination and its implications for the CMB power spectrum.

One unresolved issue that was discussed extensively in the 1990s is whether hydrogen photoionization can destroy photons in the He I $n^1P^o - 1^1S$ resonances (in particular, $2^1P^o - 1^1S$) and the He I 1^1S continuum, pushing He I recombination closer to Saha equilibrium. This effect was ignored in the earliest work on helium recombination [30], however Hu *et al.* [53] argued that the effect was strong enough to force helium into Saha equilibrium [50]. The argument is essentially that the time scale for the absorption of these photons is much less than the Hubble time. On the other hand, Seager *et al.* [27] argued that hydrogen photoionization was negligible because the rate of He I line excitation was much faster than the rate of H I photoionization. We show here that both of these arguments are too simple: the effectiveness of H I opacity depends not only on the optical depth per Hubble time from H I, but also on the width of the He I line and the redistribution of photons within the line. We have therefore supplemented our level code with a radiative transfer analysis of the He I lines that takes account of H I continuum opacity and emission/absorption of resonance radiation, including coherent scattering. The result is that H I opacity has little effect at $z > 2200$, because even though the H I optical depth per Hubble time can be $\gg 1$, the H I optical depth within the width of any individual He I line is small, so the standard Sobolev escape rate is unmodified and recombination proceeds similarly to Seager *et al.* [27]. At lower redshifts the exponentially increasing H I abundance begins to absorb photons out of the He I $2^1P^o - 1^1S$ line, rapidly accelerating He I recombination and leading to its completion by $z \sim 1800$.

Leung *et al.* [42] argued that the heating due to the 13.6 eV energy release per H I recombination would increase the matter temperature and thus slightly delay recombination. However this energy release couples inefficiently to the matter because it is delivered almost entirely to the photons, which are not absorbed by the matter [45]. This energy actually goes into the spectral distortion to the CMB, not the matter. In order to properly follow the matter temperature during recombination it is necessary to directly keep track of the changes in the total energy in translational degrees of freedom, and the number of such degrees of freedom (which decreases during recombination); the ratio of these quantities is $k_B T_m/2$. This was done by Seager *et al.* [27], and we do not believe any modification of the basic methodology is necessary.

Finally, the feedback of radiation field distortions from resonances onto lower-lying resonances is expected to slow recombination rates [27,48]. For example, escaped radiation from Ly β in H I could redshift onto the Ly α transition and excite atoms; analogous effects occur in He I (and in He II, although this case is less important for CMB anisotropies). This is included iteratively in the level code developed here.

In this paper, we will develop the effects through several sections. The multilevel atom code is described in Sec. II. We introduce H I continuum opacity and its effects on radiative transfer between He I lines in Sec. III. Section IV discusses an analytic approach to transport with complete redistribution and continuous (H I) opacity. Section V expands this treatment to include partial redistribution using a Monte Carlo simulation. We conclude in Sec. VI. In Appendix A we discuss the atomic data used here; Appendix II describes issues with transport under complete redistribution; and Appendix C describes our implementation of the Monte Carlo method for solving line profiles with coherent scattering. Appendix D examines the limiting cases in which the Monte Carlo method reduces to the method of Sec. IV and to the widely used Sobolev escape probability method. Finally, Appendix E describes the handling of photons above the He I photoionization threshold (24.6 eV) in our code.

II. A NEW LEVEL CODE WITH RADIATIVE FEEDBACK

The standard recombination scenario discussed in this paper is a homogeneous, interacting gas of protons, helium nuclei, electrons, and photons in an expanding background. The background dynamics (i.e. the Friedmann equation) are allowed to include other homogeneously distributed components (e.g. neutrinos, dark matter, and dark energy) but in our treatment we only consider their effect on $H(z)$, neglecting any direct interaction with the baryons and photons. Several extensions to this standard scenario have been proposed but will not be considered here: energy injection from self-annihilating or decaying dark matter, primordial magnetic fields, small-scale inhomogeneities or peculiar velocities, and others [54–63]. The underlying physics in the standard problem is known, but the solution is complicated by the interactions between radiation and atomic level occupations, and the variety of atomic rates. Many atomic rates involved are time consuming to calculate, or not known well (for example, collisional and intercombination rates in He I.) Collisional processes contribute to a lesser extent because of the high photon to baryon ratio during recombination. These are discussed in Paper III, where we argue that they are unimportant for helium recombination; in this paper we restrict ourselves to radiative processes.

Recombination calculations must ultimately meet the practical constraint that they be fast enough (running in a few seconds) to act as inputs to CMB anisotropy codes. The general procedure for developing a recombination code that meets this constraint is to first “oversimulate” the recombination history, and prioritize the effects. One then develops a practical method that encapsulates the important physics. Additional effects can be included as parametrized corrections to the model. The TLA approximation has been practical for CMB studies to date, and a

constant correction factor is sufficient to bring it into agreement with more complete methods [27]. CMB researchers have been lucky that such a fast approximation is possible, but in the post-WMAP era it is not clear whether the TLA approximation will be sufficiently accurate. Tighter experimental constraints on the high CMB multipoles in the Silk damping region will need to be matched by confidence that the underlying recombination physics is well understood. Here, we use a multilevel atom code similar to Seager *et al.* [27] to assess the significance of several new processes relative to a base model with one set of cosmological parameters. This level of detail is essential to developing an understanding of new physical effects. Unfortunately, it leads to a code that is much too slow for direct incorporation into Boltzmann codes. Developing and extension to the TLA approximation (or a similarly fast model) for a range of cosmological parameters will be the subject of later work.

Many of the important details in the calculations are wrapped up in the notation, so we present the major symbols used here in Table I.

A. Summary of the method

For brevity, we will only highlight the physical arguments of the multilevel code, and differences from Seager *et al.* [27]. The multilevel atom code tracks levels up to a maximum principal quantum number n_{\max} . In this paper, we use a smaller model for H I with 245 levels (up to $n_{\max} = 200$), He I, 289 levels ($n_{\max} = 100$), and for He II, 145 levels ($n_{\max} = 100$), resolving l sublevels up to $n = 10$, and including quadrupole and intercombination transitions in the He I rates. (A detailed discussion of atomic data can be found in Appendix A. In Paper III, we investigate the effect of changing n_{\max} and find that these can be neglected here.) Unless stated otherwise, we assume a Λ CDM cosmology with $\Omega_b = 0.04592$, $\Omega_m = 0.27$, $\Omega_r = 8.23 \times 10^{-5}$, zero spatial curvature, massless neutrinos, a Hubble parameter of $h = 0.71$, and presentday radiation temperature $T_r(z=0) = 2.728$ K. The fiducial fractional helium abundance (i.e. ratio of helium to hydrogen nuclei) is $f_{\text{He}} = 0.079$. The Hubble rate in such a cosmology is

$$H(z) = H_0 \sqrt{\Omega_\Lambda + \Omega_m(1+z)^3 + \Omega_r(1+z)^4}. \quad (1)$$

The number density of hydrogen nuclei is given by [27,36]

$$n_{\text{H}}(z) = 1.123 \times 10^{-5} \frac{\Omega_b h^2}{1 + 3.9715 f_{\text{He}}} (1+z)^3 \text{ cm}^{-3}, \quad (2)$$

where 3.9715 is the ratio of atomic masses of ^4He and ^1H . We will use the photon phase space density $\mathcal{N}(\nu)$ to track the radiation spectrum instead of the specific intensity J_ν , because the former is conserved along a trajectory in free space whereas J_ν decreases as the universe expands. The relation between these is

$$\mathcal{N}(\nu) = \frac{c^2}{2h\nu^3} J_\nu. \quad (3)$$

Photoionization and recombination contributions to atomic level population dynamics are discussed in Seager *et al.* [27], and we follow their treatment here. The rate of change of the average occupation of an atomic level is given by a series of bound-bound and bound-free rate equations. The photoionization rate from some level i is given by

$$\beta_i = \frac{8\pi}{c^2} \int_{\nu_{\text{th},i}}^{\infty} \sigma_{ic}(\nu) \nu^2 \mathcal{N}(\nu) d\nu, \quad (4)$$

where $\mathcal{N}(\nu)$ is the photon phase space density, ν_{th} is the photoionization threshold frequency from level i , and σ_{ic} is the photoionization cross section from that level, as a function of frequency (implicit in subsequent equations). The photorecombination rate density for spontaneous and stimulated processes is

$$\alpha_i = \frac{8\pi}{c^2} \left(\frac{n_i}{n_e n_c} \right)^{\text{LTE}} \int_{\nu_{\text{th},i}}^{\infty} \sigma_{ic} \nu^2 [1 + \mathcal{N}(\nu)] e^{-h\nu/k_B T_m} d\nu, \quad (5)$$

where T_m is the matter temperature. The prefactor is the Saha ratio of the occupation of the level i (in local thermal equilibrium, LTE) to the free electron density times the continuum state density,

$$\left(\frac{n_i}{n_e n_c} \right)^{\text{LTE}} = \left(\frac{h^2}{2\pi m_e k_B T_m} \right)^{3/2} \frac{g_i}{2g_c} e^{h\nu_{\text{th}}/k_B T_m}, \quad (6)$$

where i labels a bound state of a species, and c labels the continuum state (e.g. for hydrogen this is H II) of the species; g_i and g_c are the state degeneracies. The bound-free rate for a level i is then

$$\frac{dx_i}{dt} = \alpha_i n_e x_c - \beta_i x_i. \quad (7)$$

Except for several transitions in He I where transport is calculated separately to include new effects, single photon bound-bound rates are calculated in the standard Sobolev approximation with complete redistribution,

$$\frac{dx}{dt} = A_{u \rightarrow l} P_S \left[x_u (1 + \mathcal{N}_+) - \frac{g_u}{g_l} x_l \mathcal{N}_+ \right], \quad (8)$$

where $A_{u \rightarrow l}$ is the Einstein rate coefficient connecting an upper bound state u to a lower bound state l , and \mathcal{N}_+ is the phase space density of radiation on the blue side of the line. In the ‘‘original’’ version of the code (i.e. before feedback is included) this is taken to be the Planck distribution, $\mathcal{N}_+ = \mathcal{N}_{\text{pl}} = (e^{h\nu/k_B T_r} - 1)^{-1}$. In the Sobolev approximation, the rates are modulated by the probability that a photon will escape from the resonance, allowing the average occupation state of the gas to change. The probability is associated with the Sobolev effective optical depth,

TABLE I. Symbols used in this paper. Units of “1” mean the quantity is dimensionless.

Symbol	Units	Description	Equation
a	1	Voigt unitless width parameter	Eq. (C5)
$A_{i \rightarrow j}$	s^{-1}	Einstein spontaneous one-photon decay rate for i to j	
f_{coh}	1	fraction of line photon absorptions resulting in coherent scattering	
f_i	1	fraction of line photon absorptions followed by transition to level i	
f_{inc}	1	fraction of line photon absorptions resulting in incoherent processes	$f_{\text{inc}} = 1 - f_{\text{coh}}$
g_i	1	degeneracy of level i , not including nuclear spin	
H	s^{-1}	Hubble rate	
K	$\text{cm}^3 \text{s}$	Peebles K -factor [28]	$K = \lambda_{\text{line}}^3 / 8\pi H$
n_e	cm^{-3}	electron density	
n_i	cm^{-3}	density of atoms in level i	
n_{H}	cm^{-3}	total density of all hydrogen nuclei	
\mathcal{N}	1	photon phase space density	Eq. (3)
\mathcal{N}_{C}	1	\mathcal{N} in equilibrium with the continuum opacity	Eq. (41)
\mathcal{N}_{L}	1	\mathcal{N} in equilibrium with the line opacity	Eq. (22)
$\mathcal{N}_{\text{L}}^{(0)}$	1	modification of \mathcal{N}_{L} used with coherent scattering	Eq. (74)
\mathcal{N}_{PI}	1	photon phase space density for blackbody distribution	$\mathcal{N}_{\text{PI}} = 1 / (e^{h\nu/k_{\text{B}}T_{\text{r}}} - 1)$
\mathcal{N}_{\pm}	1	photon phase space density on the blue (+) or red (-) side of a line	Eq. (25)
$\bar{\mathcal{N}}$	1	photon phase space density averaged over the profile	Eq. (50)
P_{C}	1	probability of photon emitted in line being absorbed by H I	Eq. (53)
P_{esc}	1	escape probability from the line (equal to P_{S} in Sobolev approximation)	
P_{MC}	1	prob. of photon in MC being lost by H I absorption or redshifting	
P_{S}	1	Sobolev escape probability	Eq. (10)
\mathcal{Q}	erg s^{-1}	heating per hydrogen nucleus per unit time	
R_{ij}	s^{-1}	transition rate from level i to level j	
$T_{\text{m}}, T_{\text{r}}$	K	matter (T_{m}) or radiation (T_{r}) temperature	
x	1	frequency relative to line center in Doppler units	$x = (\nu - \nu_{\text{line}}) / \Delta\nu_{\text{D}}$
x_e	1	abundance of electrons relative to total hydrogen nuclei	$x_e = n_e / n_{\text{H}}$
x_i	1	abundance of the state i relative to total hydrogen nuclei	$x_i = n_i / n_{\text{H}}$
x_{tot}	1	total number of free particles per hydrogen nucleus	
α_i	$\text{cm}^3 \text{s}^{-1}$	recombination coefficient to level i	
β_i	s^{-1}	photoionization rate from level i	
Γ_i	s^{-1}	width of level i	
Γ_{line}	s^{-1}	Lorentz width of the line	
$\Gamma_{\mathcal{Q}}$	$\text{erg cm}^{-3} \text{s}^{-1}$	heating rate per hydrogen nucleus	
$\Delta\nu_{\text{D}}$	Hz	Doppler width of line	
η_{c}	Hz^{-1}	differential optical depth from continuous opacity	Eq. (27)
$\Lambda_{i \rightarrow j}$	s^{-1}	spontaneous two-photon decay rate from i to j	
$\Lambda_{\mathcal{Q}}$	$\text{erg cm}^{-3} \text{s}^{-1}$	cooling rate per hydrogen nucleus	
$\nu_{\text{line}}, \nu_{ul}$	Hz	frequency of line center; ν_{ul} for specific upper and lower levels	
$\nu_{\text{th},i}$	Hz	photoionization threshold frequency from level i	
ξ	1	rescaled photon phase space density	Eq. (76)
Π	Hz^{-1}	Monte Carlo method probability distribution of photon frequency	
σ_{ic}	cm^2	photoionization cross section from level i	
σ_{T}	cm^2	Thomson cross section	
τ_{coh}	1	Sobolev optical depth from coherent scattering	$\tau_{\text{coh}} = f_{\text{coh}} \tau_{\text{S}}$
τ_{inc}	1	Sobolev optical depth from incoherent processes	$\tau_{\text{inc}} = f_{\text{inc}} \tau_{\text{S}}$
τ_{LL}	1	optical depth from continuous opacity between lines	Eq. (30)
τ_{S}	1	total Sobolev optical depth	Eq. (9)
ϕ	Hz^{-1}	atomic line profile	
χ	1	photon-atom scattering angle	Eq. (C1)

$$\tau_S = \frac{A_{u \rightarrow l} c^3}{8\pi H(z) \nu_{ul}^3} n_H \left(x_l \frac{g_u}{g_l} - x_u \right), \quad (9)$$

so that

$$P_S = \frac{1 - e^{-\tau_S}}{\tau_S}. \quad (10)$$

B. Matter temperature

The matter temperature, T_m , departs from the radiation temperature due to adiabatic expansion, Compton cooling, free-free, bound-free, and bound-bound processes [27]. Here, we write the heat exchange terms to emphasize the individual processes, kinetic degrees of freedom in the gas, and we expand the description of free-free processes in [27]. Nothing is fundamentally new or unexpected in this treatment, and, indeed, we find that the departure of T_m from T_r is negligible during He I recombination. The rate of change of the matter temperature is related to the heating/cooling processes and adiabatic expansion in the gas through

$$\dot{T}_m = \frac{2}{3k_B x_{\text{tot}}} (\mathcal{Q}_{\text{es}} + \mathcal{Q}_{\text{ff}} + \mathcal{Q}_{\text{bf}} + \mathcal{Q}_{\text{bb}}) - 2HT_m, \quad (11)$$

where the “es” subscript denotes Compton cooling and the others denote radiative atomic processes between bound and free levels. An individual heat exchange process \mathcal{Q} has the general form

$$\mathcal{Q} = \frac{\Gamma_{\mathcal{Q}} - \Lambda_{\mathcal{Q}}}{n_H} - \frac{3}{2} \dot{x}_{\text{tot}} k_B T_m, \quad (12)$$

where $\Gamma_{\mathcal{Q}}$ and $\Lambda_{\mathcal{Q}}$ are the heating and cooling rates (in $\text{erg cm}^{-3} \text{s}^{-1}$), and \dot{x}_{tot} accounts for processes that modify the number of kinetic particles in the gas. The Compton (electron scattering) cooling term is

$$\mathcal{Q}_{\text{es}} = -4x_e c \sigma_T a_R T_r^4 \frac{k_B (T_r - T_m)}{m_e c^2}, \quad (13)$$

where we have used the radiation constant $a_R = \pi^2 k_B^4 / 15c^3 \hbar^3$. The free-free contribution to \dot{T}_m is the integral of the free-free opacity over the radiation temperature blackbody distribution (heating) minus the matter temperature blackbody distribution (cooling),

$$\mathcal{Q}_{\text{ff}} = \frac{8\pi}{n_H c^2} \int \nu^2 [\mathcal{N}_{\text{Pl}}(\nu, T_r) - \mathcal{N}_{\text{Pl}}(\nu, T_m)] h\nu \alpha_{\text{ff}}(\nu) d\nu, \quad (14)$$

where \mathcal{N}_{Pl} is the blackbody distribution, and the length absorption coefficient $\alpha_{\text{ff}}(\nu)$ in units of cm^{-1} is [64]

$$\alpha_{\text{ff}}(\nu) = \frac{4e^6}{3m_e h c} \sqrt{\frac{2\pi}{3k_B m_e}} T_m^{-1/2} \nu^{-3} n_e n_{\text{HII}} \times (1 - e^{-h\nu/k_B T_m}) \bar{g}_{\text{ff}}. \quad (15)$$

The thermally averaged Gaunt factor \bar{g}_{ff} is given by Sutherland [65]. In principle there is an additional correction due to free-free radiation from electron-He II and electron-He III collisions, however these other species are an order of magnitude less abundant than H II, and deviations from $T_m = T_r$ are negligible for helium recombination, regardless. Therefore we have not included helium free-free radiation in our matter temperature evolution.

The bound-free contribution to \dot{T}_m is from energy exchanged in photorecombination and photoionization, and due to the change in x_{tot} ,

$$\mathcal{Q}_{\text{bf}} = \sum_i \left[\left(\frac{\Gamma_{\mathcal{Q},i}}{n_H} - \frac{3}{2} \beta_i x_i k_B T_m \right) - \left(\frac{\Lambda_{\mathcal{Q},i}}{n_H} - \frac{3}{2} \alpha_i n_e x_c k_B T_m \right) \right]. \quad (16)$$

The energy exchanged per bound-free process includes the heating due to photoionization,

$$\frac{\Gamma_{\mathcal{Q},i}}{n_H} = x_i \frac{8\pi}{c^2} \int_{\nu_{\text{th},i}}^{\infty} \sigma_{ic} \nu^2 \mathcal{N}(\nu) h(\nu - \nu_{\text{th},i}) d\nu, \quad (17)$$

and the cooling due to recombination,

$$\frac{\Lambda_{\mathcal{Q},i}}{n_H} = n_e x_c \frac{8\pi}{c^2} \left(\frac{n_i}{n_e n_c} \right)^{\text{LTE}} \int_{\nu_{\text{th},i}}^{\infty} \sigma_{ic} \nu^2 [1 + \mathcal{N}(\nu)] \times h(\nu - \nu_{\text{th},i}) d\nu. \quad (18)$$

We have computed these results using the blackbody function for $\mathcal{N}(\nu)$, since it is the thermal CMB photons that are responsible for the photoionizations and stimulated recombinations in the Balmer, Paschen, etc. continua of H I, and the analogous continua of He I. The potential pitfall in this assumption is that some of the photons emitted in the He I 21.2 eV line ($2^1 P^o - 1^1 S$) photoionize H I directly from the $1s$ level. This provides an additional source of heating during helium recombination that is not included in our code. However a simple calculation shows that it is negligible. The maximum amount of thermal energy that can be injected by such photons is $21.2 - 13.6 = 7.6$ eV per photon. Since a fraction $f_{\text{He}}/x_{\text{tot}} \sim 0.04$ of the matter particles during this era are heliums (He I or He II), this implies an injected energy of ~ 0.3 eV per particle, even assuming every helium recombination injects the maximum amount of energy. For comparison the total energy in translational modes of the matter is $(3/2)k_B T_m = 0.6$ eV per particle. Even at the very end of helium recombination, the Compton cooling time is

$$\begin{aligned}
 t_{\text{Compton}} &= \frac{(3/2)x_{\text{tot}}k_B(T_m - T_r)}{Q_{\text{es}}} = \frac{3x_{\text{tot}}m_e c}{8x_e \sigma_T a_R T_r^4} \\
 &\approx 7 \times 10^6 \text{ s};
 \end{aligned}
 \tag{19}$$

in comparison, the time scale for helium to recombine is several times 10^{12} s. The maximum fractional change in the matter temperature is then $0.3 \text{ eV}/0.6 \text{ eV}$ multiplied by the ratio of the Compton cooling to recombination time, which is of order 10^{-6} . This can be neglected.

The contribution from bound-bound transitions (Q_{bb}) is negligible through a similar argument. Bound-bound processes do not change x_{tot} , so the term Q_{bb} is determined by the average amount of energy delivered to the gas by a photon that is injected into (or redshifts onto) a resonance line. In general, the net heating rate can only be calculated by a detailed radiative transfer analysis [66]. However, as we saw in the previous paragraph, the injection of energy changes T_m at the 10^{-6} level if each He I recombination releases 7.6 eV of energy into the gas. Since there is a total of 24.6 eV available per He I recombination, T_m would change by only several parts in 10^6 even if *all* of this energy were released into the gas by resonance line scattering. Therefore we can neglect the bound-bound contribution to T_m .

Time derivatives for the occupations and temperatures are converted to redshift derivatives according to

$$\frac{dz}{dt} = -(1+z)H(z).
 \tag{20}$$

Equations (7), (8), and (11) give a set of stiff equations for the level occupations, as in Seager *et al.* [27] that can be

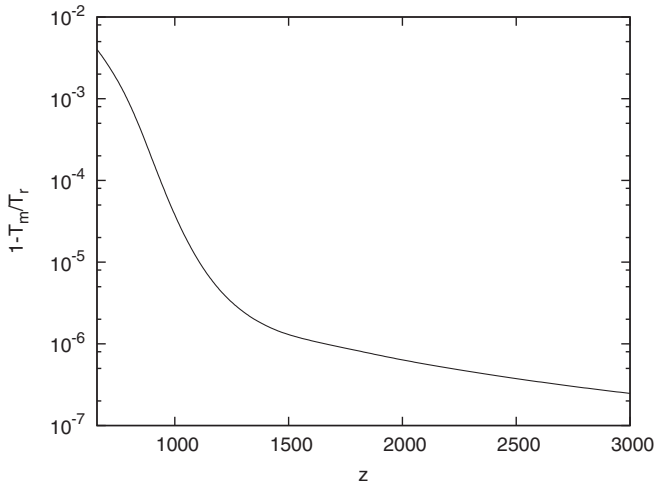


FIG. 2. The fractional difference in the matter temperature relative to the radiation temperature, $1 - T_m/T_r$. Note the sign: matter is cooler than radiation at late times because of its different adiabatic index ($5/3$ versus $4/3$). During He I recombination for $1600 < z < 3000$, the fractional difference is $< 10^{-6}$.

solved using the semi-implicit extrapolation (Bader-Deuffhard) method [67].

Our matter temperature evolution is shown in Fig. 2. The important conclusion is that the fractional temperature difference $(T_r - T_m)/T_r$ is negligible throughout helium recombination ($z \geq 1600$). This is in accord with the methods and results of Seager *et al.* [27]. At low redshifts when hydrogen recombines the matter and radiation temperatures fall out of equilibrium, but that era is not the subject of this paper.

C. Feedback

Photons that escape a high-lying resonance will readily redshift to a lower-lying line owing to the (nearly) negligible optical depth between lines. This will excite the lower-lying state, and suppress the overall formation rate of the ground state. This radiation is manifest as a spectral distortion to the thermal spectrum of radiation incident on the blue side of the lines. (The calculation shares some similarity to [68] where we showed that the relic recombination radiation is enough to ionize most of the neutral lithium population in the era following recombination, except here the radiation is fed back onto recombination.)

Feedback between levels can be calculated in a number of ways. The most direct way is to simulate a frequency-discretized radiation field along with the atomic levels. In this method, the evolution of the radiation field bins and the evolution of the occupation states of the atoms are solved for simultaneously. This is numerically very difficult. Because of the huge range of rate scales in the system and the large number of radiation bins that it is necessary to track, this method quickly becomes difficult to manage and ill-conditioned. For this reason, we use an iterative method to include feedback in the level code. This is both practical to implement, and accurate.

The level code calculates the radiation distortions generated by transitions from excited states to the ground state in a first pass, for each redshift step, for each species. The first pass assumes a blackbody radiation with local distortions in the Sobolev approximation. In a second pass, we transport the distortion generated by the $(i+1)$ th transition to the i th transition to the ground state of the same species. That is, we only transport the radiation from the next higher-lying ground-excited transition, in the same species. (Interspecies feedback between He I and H I is discussed in depth in subsequent sections.) The distortion is recalculated for each level in the second pass, and these are transported to the lower levels and applied to a third pass of the level code. The iteration continues in this way. Because the iteration step accounts for much of the total feedback effect, subsequent iterations give progressively smaller corrections, and the procedure converges rapidly. The typical fractional contribution of the fifth iteration is $|\Delta x_e| \approx 2 \times 10^{-4}$ —we stop there.

For hydrogen, the distortion is determined by a simple vacuum transport equation for one resonance. In helium,

the problem is complicated by continuous opacity from H I photoionization. Here, distortion photons are absorbed by H I in flight, and may not redshift down to the lower level. This is treated in Sec. III B.

The radiation phase space density is convenient for cosmological calculations because it is conserved along a ray, yielding the bound-bound transport equation for complete redistribution (here for H I),

$$\begin{aligned} \frac{\partial \mathcal{N}}{\partial \nu} &= \tau_S \phi(\nu) [\mathcal{N}(\nu) - \mathcal{N}_L] \\ &\approx \tau_S \phi(\nu) \left[\mathcal{N}(\nu) - \frac{x_u g_l}{x_l g_u} \right], \end{aligned} \quad (21)$$

where \mathcal{N}_L is the radiation phase space density that would be in equilibrium with the line,

$$\mathcal{N}_L = \frac{x_u}{x_l(g_u/g_l) - x_u} \approx \frac{x_u g_l}{x_l g_u}. \quad (22)$$

[This is obtained by setting the deexcitation rate $A_{u \rightarrow l}(1 + \mathcal{N})$ equal to the excitation rate $g_u A_{u \rightarrow l} \mathcal{N} / g_l$.] Here we have used the approximation that the upper level is significantly less occupied than the lower level, which is valid when the lower level is the ground state since the energy of the first excitation in H I, He I, or He II is many times $k_B T_r$. The transport equation has the solution

$$\mathcal{N}(\nu) = \frac{x_u g_l}{x_l g_u} - C \exp \left[-\tau_S \int_{\nu}^{\infty} \phi(\nu) d\nu \right], \quad (23)$$

where C is the constant of integration. This constant is obtained from the initial condition that the far blue side of the line has some phase space density \mathcal{N}_+ , which implies

$$C = \frac{x_u g_l}{x_l g_u} - \mathcal{N}_+. \quad (24)$$

Thus the phase space density \mathcal{N}_- on the red side of the line is

$$\mathcal{N}_- = \mathcal{N}_+ + \left(\frac{x_u g_l}{x_l g_u} - \mathcal{N}_+ \right) (1 - e^{-\tau_S}). \quad (25)$$

Notice that as τ_S becomes very large, the phase space density on the red side of the line approaches \mathcal{N}_L . Because \mathcal{N} is conserved during the transport between H I and He II resonances (i.e. there is negligible continuum absorption or emission), the phase space density on the blue side of the H I Ly n resonance (i.e. $1s - np$) is simply the phase space density on the red side of the Ly $(n+1)$ resonance at an earlier time:

$$\begin{aligned} \mathcal{N}_+(Ly_n, z) &= \mathcal{N}_-[Ly_{n+1}, z'], \\ z' &= \frac{1 - (n+1)^{-2}}{1 - n^{-2}} (1 + z) - 1, \end{aligned} \quad (26)$$

where $[1 - (n+1)^{-2}]/[1 - n^{-2}]$ is the ratio of line frequencies. A similar result holds for He II. Because of the existence of H I continuum opacity during He I recombi-

nation, this result does not apply to He I; we will treat the He I problem in Sec. III.

III. HYDROGEN CONTINUUM OPACITY AND HELIUM RECOMBINATION

One of the major issues in recombination physics during the 1990s was whether helium recombines in Saha equilibrium, or is delayed. On the one hand, studies by Seager *et al.* [27] and Matsuda *et al.* [30,31] found that there is an “ $n = 2$ bottleneck” in which He I recombines slowly because the two-photon $2^1S - 1^1S$ transition is slow and the $2^1P^o - 1^1S$ line is extremely optically thick; hence an excited helium atom has only a low probability of reaching the ground state and is most likely to be reionized by the CMB. These studies thus found a slower-than-Case B recombination for He I (where the $n^1P^o - 1^1S$ transitions are optically thick [69] and processes that depopulate a level through $n^1P^o - 1^1S$ are “blocked” by absorption of the same quanta, on average, thus greatly suppressing electron capture followed by direct cascade to the ground state). On the other hand, there is some neutral hydrogen present during the helium recombination era, and Hu *et al.* [53] argued that this can speed up helium recombination by absorbing resonance line and continuum photons that would otherwise excite or ionize He I. There appears to be no satisfactory explanation in the literature for why the more recent works do not agree, but the difference in CMB spectra is several percent at high ℓ [27] so it is essential that the issue be resolved. This section, as well as Secs. IV and V, are devoted to this issue.

There are fundamentally three ways that H I continuous opacity could speed up He I recombination:

- (1) Hydrogen can suppress feedback in the He I lines by absorbing He I line radiation before it redshifts down to the next line and excites a helium atom.
- (2) If the H I opacity is very large, it could directly absorb He I resonance line photons, thus increasing the effective line escape probability above its Sobolev value.
- (3) Sometimes a helium atom recombines directly to the ground state. In the case of hydrogen, such recombinations are ineffective because the emitted photon immediately ionizes another atom. However in the case of helium, it is possible to produce a neutral helium atom but have the emitted photon ionize an H I atom instead of He I. This results in a net recombination of helium.

We treat mechanism #1 in Secs. III A and III B. The problem of absorption of He I line photons by H I (mechanism #2) is more complicated. The physical picture is outlined in Sec. III C, and it is split into two cases. For the helium intercombination and quadrupole lines, there is negligible coherent scattering within the line since the upper level has allowed decays (and allowed pathways to other states) whereas reemission of the photon to the

ground state of He I is semiforbidden or forbidden. This case is the simplest to consider and it is treated analytically in Sec. IV. The other case is that of the allowed He I $n^1P^o - 1^1S$ lines, in which coherent scattering plays a key role alongside incoherent absorption/emission processes and H I opacity in determining the line profile and net decay rate. This situation is treated via Monte Carlo simulation in Sec. V. Mechanism #3 produces a negligible effect and so we discuss it in Appendix E. We will develop the distinction between coherent scattering and incoherent processes much more carefully in Sec. III C and VA.

A. Continuum opacity

The photons emitted in resonant transitions in He I from excited states to the ground state have energies above the H I photoionization threshold. The opacity from photoionization influences transport both within and between He I lines. In this section, we describe how the continuum opacity is calculated, and Secs. IV and V describe details of transport subject to continuous opacity. Throughout, we use η_c to represent the continuum depth per unit frequency,

$$\eta_c = \left. \frac{d\tau}{d\nu} \right|_{\text{continuum}} = \frac{n_{\text{H}} x_{1s} \sigma_{c1} c}{H\nu}, \quad (27)$$

where σ_{c1} is the photoionization cross section of neutral hydrogen, and x_{1s} is the ground state occupation fraction (the excited states have much lower occupation numbers and lower photoionization cross sections, so we neglect them). Stimulated recombination to H($1s$) can be neglected. The continuum optical depth is also slowly varying as a function of frequency for the He I ground-resonance transitions because the energies are above the H I photoionization threshold and single-electron atoms such as H I possess no multiple-excitation resonances in their cross section.

In standard recombination theory, the neutral hydrogen population is well described by the Saha distribution at early times ($z > 1700$):

$$x_{\text{HI}} \approx x_e x_{\text{HII}} n_{\text{H}} \left(\frac{h^2}{2\pi m_e k_{\text{B}} T_{\text{m}}} \right)^{3/2} e^{x_{\text{HI}}/k_{\text{B}} T_{\text{m}}}, \quad (28)$$

where $x_{\text{HII}} = 1 - x_{\text{HI}} \approx 1$. One concern in using this equation to estimate the effect on helium recombination is that radiation from helium recombination could knock the neutral hydrogen population out of equilibrium. This would tend to lower the neutral hydrogen population, and decrease the continuum opacity. In the worst case, each He I recombination photoionizes a hydrogen atom, giving the characteristic time scale for ionization, $t_{\text{ionize}} \approx x_{\text{HI}}/\dot{x}_{\text{HeI}}$. The Saha relaxation time for this perturbation to fall back to Saha equilibrium is well approximated by the time scale for perturbations to decay in the TLA approximation (neglecting the H I recombination rate at these high redshifts),

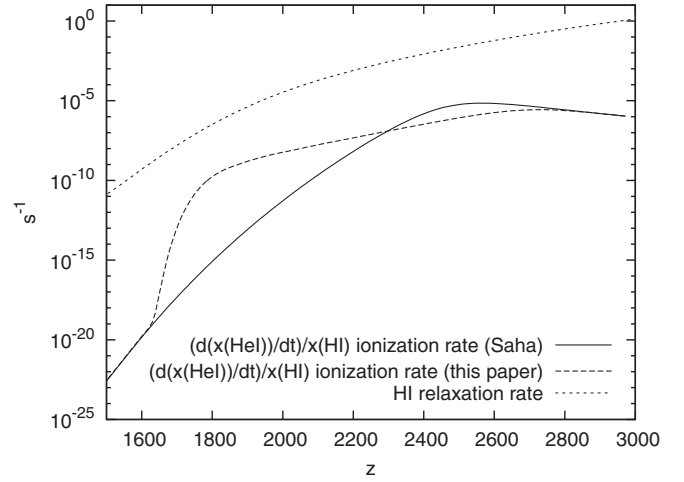


FIG. 3. The ionization/relaxation timescales of H I during the period of He I recombination, assuming each He I recombination generates a photon that photoionizes a hydrogen atom. Here we consider two He I recombination histories: one in equilibrium and the history derived here (Fig. 12). The ‘‘H I relaxation rate’’ is the inverse-time scale t_{Saha}^{-1} (Eq. (29)) for H I to return to Saha equilibrium if its abundance is perturbed. In either He I history, the ionizing radiation from He I is not sufficient to push H I evolution out of Saha equilibrium.

$$t_{\text{Saha}} \approx \frac{\beta_{\text{H}} + \Lambda_{2s \rightarrow 1s} + (K n_{\text{H}} x_{\text{HI}})^{-1}}{\Lambda_{2s \rightarrow 1s} + (K n_{\text{H}} x_{\text{HI}})^{-1}} \frac{1}{\beta_{\text{H}}} e^{E_{2p \rightarrow 1s}/k_{\text{B}} T}, \quad (29)$$

where $K = \lambda_{\text{Ly}\alpha}^3/8\pi H$ is the Peebles K -factor [28] and β_{H} is the effective hydrogen photoionization coefficient from $n = 2$ in the three-level approximation. These are calculated, and shown for comparison in Fig. 3. It is evident that a perturbation to the neutral hydrogen population caused by He I photoionizing radiation quickly relaxes back to the Saha evolution.

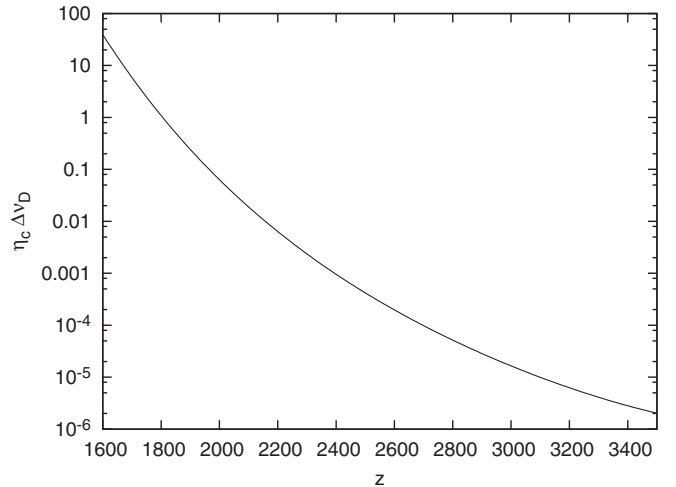


FIG. 4. The continuum optical depth $d\tau_c/d\nu = \eta_c$ times the Doppler width of He I $2^1P^o - 1^1S$ as a function of redshift.

The unitless quantity $\eta_c \Delta \nu_D$ (where $\Delta \nu_D$ is the ^4He Doppler width) during the He I recombination era is shown in Fig. 4.

The energy separations between transitions from excited states to the ground state in He I are typically much greater than the optically thick linewidth. Thus, radiative transport in He I can be thought of as taking place through two phases. In the first, continuum processes influence transport within a line. This modifies the transition rates, and sets the escape probability from a given resonance, which may exceed the Sobolev value. This is described in Sec. III C. In a second phase, continuum processes influence the transport of radiation between resonances, as described in the next section.

B. Feedback from transport between He I lines and continuous opacity

Section II C addressed the feedback of a radiation distortion produced by a higher resonance on lower-lying resonances in H I and He II. For H I and He II, this transport is in free space in the approximation that the resonances are spaced more widely than their widths. (This approximation is not entirely valid for H I at late times, however this is not relevant to helium recombination and will be deferred to a later paper.) In He I, the picture is more complicated because transport is subject to opacity from the photoionization of neutral hydrogen. There is a sufficient neutral population that, when integrated over the photon's trajectory, the feedback between levels can be significantly suppressed. This is true especially near the end of the He I recombination and beginning of H I recombination.

The algorithm presented earlier to include feedback iteratively can be easily modified to include feedback suppression between lines: calculate the distortions for all resonances, and in the next iteration, multiply them by a suppression factor before applying them to the lower line. Changing variables to redshift, the total depth of the continuum between lines is

$$\tau_{LL} = \int_{z_{\text{abs}}}^{z_{\text{em}}} \frac{n_{\text{H}} \chi_{1s} \sigma_{c1} c}{H} \frac{dz}{1+z}. \quad (30)$$

Let \mathcal{N}_i be the radiation field on the blue side of the lower line assuming there is no line-line optical depth τ_{LL} . Then the nonthermal distortion produced by the higher state is \mathcal{N}_i minus the Planck spectrum (since at times earlier than $z \sim 1600$ H I is in Saha equilibrium, to a good approximation), which is suppressed by the line-line depth. The final radiation field just above the frequency of the lower-lying line is then

$$\mathcal{N}_+ = (\mathcal{N}_i - \mathcal{N}_{\text{pl}}) e^{-\tau_{LL}} + \mathcal{N}_{\text{pl}}, \quad (31)$$

where the Planck spectrum is $\mathcal{N}_{\text{pl}} = 1/(e^{h\nu/k_B T_i} - 1)$.

The effect of feedback is shown in Fig. 5, and the effect of including τ_{LL} is shown in Fig. 6.

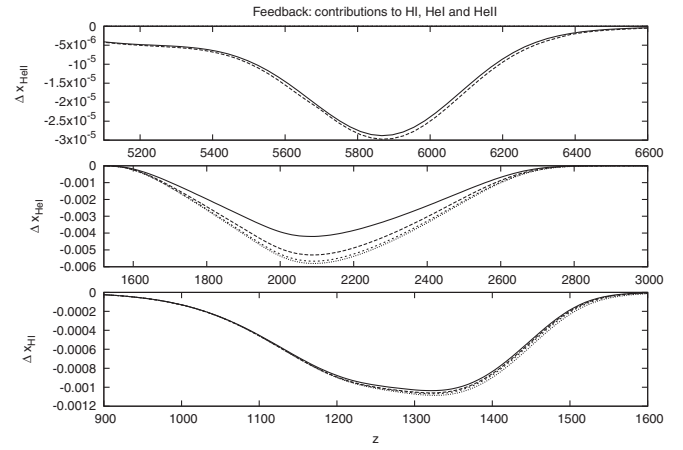


FIG. 5. A comparison of the effect of feedback of a spectral distortion produced by higher-lying states on lower-lying states in the same species after several iterations, relative to the reference model, for He II, He I, and H I, where Δx is the abundance with feedback minus without feedback. Here, continuous opacity from hydrogen photoionization between He I is included (discussed in Fig. 6). In all cases, feedback has the effect of retarding the formation of the neutral species. A larger number of iterations (~ 5) are needed for He I recombination than for H I or He II. Here, the uppermost line is the first iteration, moving down with further iterations and better convergence.

C. Transport within He I lines and continuous opacity: physical argument

Previous analyses [27,53] identify neutral hydrogen as a potential catalyst that could cause He I recombination to proceed closer to Saha equilibrium. This is because photons locked in the optically thick He I $n^1P^o - 1^1S$ lines can ionize neutral hydrogen. This removes the photons and

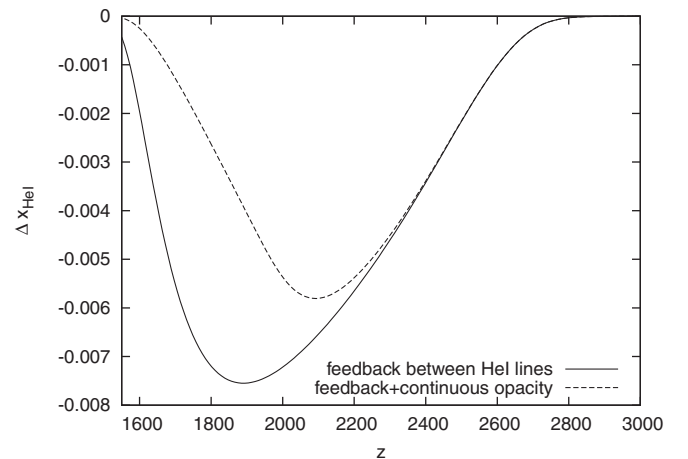


FIG. 6. The effect of hydrogen continuum absorption on the feedback between transitions to the ground state in He I. Feedback slows He I recombination, but becomes increasingly less significant as more hydrogen recombines, increasing the bound-free opacity and absorbing the distortion.

thus prevents them from reexciting a helium atom:

$$\text{He}(n^1P^o) \rightarrow \text{He}(1^1S) + \gamma, \quad \text{H}(1s) + \gamma \rightarrow \text{H}^+ + e^-. \quad (32)$$

The purpose of this section is to investigate this process and related processes in the He I intercombination and quadrupole lines. We will only discuss the physical situation here, leaving the detailed calculation to Sec. IV (for intercombination and quadrupole lines) and V (for permitted lines). In those sections the objective will be to evaluate the increase in effective escape probability P_{esc} (Eq. (10)) due to H I. Before we do so, however, we must discuss the issue of coherent scattering and its implications for what is meant by the “width” of a He I line; we also provide a simple physical explanation for why H I opacity becomes important when it does (i.e. at $z \sim 2200$).

1. Coherent vs incoherent processes

Optically thick lines in cosmological recombination are usually treated by the Sobolev method (see e.g. Sec. 2.3.3 of Ref. [27] for a good discussion). This method describes decays from an excited level u of atoms to a lower level l without regard to how the atom reached the excited state. This a good approximation in the case of forbidden lines, and it is also good for very optically thick lines in the absence of other sources of opacity (in this case the radiation field in the optically thick part of the line comes to equilibrium with the population ratio of u and l , and thereafter the details of the radiative transfer matter little). However in the case of He I recombination, where He I and H I compete for photons, no equilibrium is established and the resonance line profile matters. In particular, the frequency distribution of photons emitted in e.g. $2^1P^o - 1^1S$ need not be a Voigt profile and indeed need not be the same as the absorption profile $\phi(\nu)$. The reason is that sometimes level u is populated by resonant absorption of a photon from level l , which subsequently decays back to l without any intermediate interactions. In this case, conservation of energy requires the frequency of the final photon to be the same as the frequency of the initial photon in the atom’s rest frame, and hence such events will be called “coherent scattering.” In the comoving frame the photon’s frequency undergoes a small fractional shift of order ν/c , where ν is the atomic velocity. This small frequency shift has a minor influence on recombination, and will be included in the calculation of Sec. V. For emphasis we will continue to call these scattering events coherent with the understanding that coherence is meant to be exact in the atom’s frame; this should not lead to any confusion since there is *no* type of scattering that is coherent in the comoving frame instead of the scatterer’s frame. (Note, however, that the term “coherent scattering” applied in the comoving frame does appear in literature.)

The process described above differs from “incoherent scattering” [70,71], in which the excited atom undergoes

other interactions (almost always involving one or more photons) before returning to l . It is only in the latter case that the final photon’s frequency distribution can be described by a Voigt profile (complete redistribution). It is also possible for the atom in the excited state u to become ionized, which we will consider to be an incoherent process since if the electron later recombines (probably onto another atom) the spectrum of emitted radiation will bear no memory of the frequency of the photon that initially excited the atom. Based on this distinction, one may split the Sobolev optical depth for a line into pieces: $\tau_s = \tau_{\text{coh}} + \tau_{\text{inc}}$, depending on the fractions f_{coh} and f_{inc} of photon absorptions in the lines that go to coherent or incoherent processes, respectively. Note that by classifying ionization from the excited state as an incoherent process, we ensure $f_{\text{inc}} + f_{\text{coh}} = 1$.

The practical implication of this distinction is that when solving for the phase space density $\mathcal{N}(\nu)$ across an optically thick line, incoherent processes can play a dominant role even if $f_{\text{inc}} \ll 1$, as is the case for the He I $2^1P^o - 1^1S$ line. This is because incoherent scattering can transport a photon from the line center to a far damping wing (or vice versa) in one scattering event, and an excitation followed by ionization can remove a photon from the resonance line. In contrast, coherent scattering can only move a photon far into the damping wings by taking many “baby steps” using the Doppler shift from the atom’s velocity, and it by itself cannot create or destroy a line photon. We distinguish two physically distinct cases here: one where the coherent scattering is negligible (to be studied in detail in Sec. IV) and a more complicated case of partial redistribution where it is not (Sec. V).

2. When is continuum opacity important?

The He I $2^1P^o - 1^1S$ line is in the extreme UV at 21.2 eV, where the optical depth from neutral hydrogen photoionization is nearly constant in the neighborhood of the resonance. The continuous opacity from neutral hydrogen is also present in radiation transport within the He I $n^1P^o - 1^1S$ series, [He I] $n^1D - 1^1S$, and He I] $n^3P^o - 1^1S$. Seager *et al.* [27] concluded that this effect is negligible for $2^1P^o - 1^1S$ because the neutral hydrogen photoionization rate from photons in the $2^1P^o - 1^1S$ resonance is orders of magnitude lower than the $2^1P^o - 1^1S$ photoexcitation rate during the He I recombination history, due to the sparse population of neutral hydrogen. A better criterion for the significance of neutral hydrogen is whether or not continuous opacity affects radiative transport within the line. The two natural scales in the transport problem are: (i) the frequency η_c^{-1} that a photon can be expected to traverse by redshifting before it is absorbed in a hydrogen photoionization event, and (ii) the range of frequencies $\Delta\nu_{\text{line}}$ over which the line is thick to incoherent scattering/absorption. If $\eta_c^{-1} \gg \Delta\nu_{\text{line}}$ then helium atoms will reabsorb the resonance radiation from other helium

atoms, without regard to the H I abundance. If, on the other hand, $\eta_c^{-1} \leq \Delta\nu_{\text{line}}$, then H I can destroy photons that would otherwise have reexcited helium atoms, and thereby accelerate He I recombination. We thus care about the continuum optical depth within a line,

$$\tau_C = \eta_c \Delta\nu_{\text{line}}. \quad (33)$$

In the case of lines that are optically thick into the damping wings, such as the He I $n^1P^o - 1^1S$ lines, $\Delta\nu_{\text{line}}$ may be calculated by integrating the asymptotic line profile $\phi(\nu) \sim \Gamma_{\text{line}}/4\pi^2\Delta\nu^2$ until the optical depth in the wing becomes unity:

$$\Delta\nu_{\text{line}} = \frac{\Gamma_{\text{line}}\tau_{\text{inc}}}{4\pi^2}. \quad (34)$$

Here Γ_{line} is the Lorentz width of the line, τ_{inc} is the Sobolev optical depth through the line from incoherent processes (i.e. all absorption processes other than coherent scattering; this will be calculated in Sec. V), and η_c is the differential continuum optical depth, Eq. (27). Figure 7 compares the optically thick linewidth (from incoherent processes) to the inverse differential optical depth η_c^{-1} and the Doppler width for the $2^1P^o - 1^1S$ transition in ^4He . The line may be optically thick in the Sobolev sense out to much larger frequency separations due to coherent scattering, but a coherent scattering event results in no net change in the atomic level populations and hence does not directly affect recombination. (It only has an indirect effect by changing the radiation spectrum.)

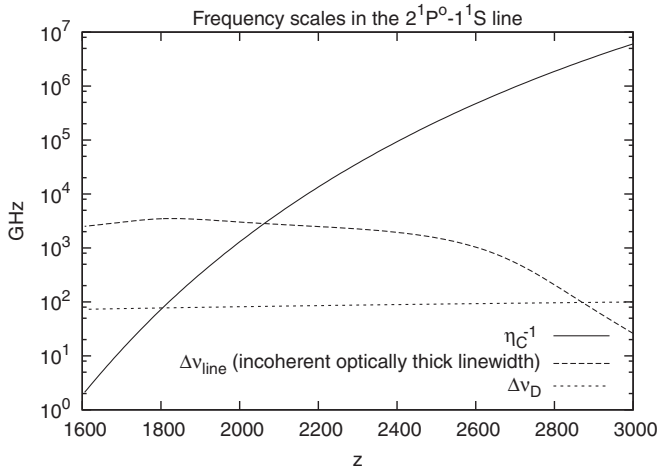


FIG. 7. Inverse of the differential optical depth η_c from hydrogen photoionization as a function of redshift, compared to the optically thick line-width due to incoherent processes in the $2^1P^o - 1^1S$ line. Continuum processes start to become important over scales inside the (incoherent) optically thick part within the line around $z = 2100$. Also plotted is the Doppler width of the line, emphasizing that the line is optically thick out into the wings. Continuum processes do not act on scales smaller than the Doppler core until $z < 1800$.

The general problem of the escape probability including the continuum opacity and coherent scattering as well as incoherent emission/absorption processes is quite complicated. Therefore we will solve it in two steps. In Sec. IV we will solve the problem *without* coherent scattering. This is a conceptually simple problem—all one has to do is compute the probability of a photon either redshifting out of the line or being absorbed by H I before being reabsorbed by He I—and the machinery for solving it has already been developed for the theory of line transfer in stellar winds [72]. Despite its simplicity, the solution in Sec. IV is an accurate description of the intercombination and quadrupole lines because there is negligible coherent scattering in these lines. (The reason is that if an atom absorbs a photon in these lines and reaches a n^3P^o or n^1D level, its next step is almost always to undergo one of the allowed decays rather than to emit a photon in the intercombination or quadrupole line and go back to the ground state.) In Sec. V we address the problem *with* coherent scattering as well as incoherent processes and continuum opacity, and describe its solution via a Monte Carlo simulation.

IV. THE MODIFIED ESCAPE PROBABILITY WITHOUT COHERENT SCATTERING

This section is concerned with calculating the net decay rate in He I lines with continuous opacity (from H I) but no coherent scattering. This is a line radiative transfer problem with “complete redistribution” in the sense that a photon emitted in the line has a frequency distribution given by the intrinsic line profile, independent of the spectrum of incident radiation:

$$p(\nu_{\text{out}}|\nu_{\text{in}}) = \phi(\nu_{\text{out}}). \quad (35)$$

There is negligible coherent scattering in the He I $n^3P^o - 1^1S$ and [He I] $n^1D - 1^1S$ lines (see Sec. III C), and results in this section are readily applied to those lines. The macroscopic picture is that in emission, a line in the gas always has the same shape, regardless of the excitation field. Throughout, ϕ is Voigt-distributed and accounts for the natural resonance width of the line and Doppler broadening from thermal motion, set by the matter temperature. In Sec. V we discuss the case of a line in a gas where some fraction of the photons are reemitted coherently (with the same frequency as the incoming photon in the rest frame of the atom) and some are reemitted incoherently.

The fundamental quantity that determines the transition rate between a lower level l and upper level u is the radiation phase space density integrated over the atomic absorption profile, $\hat{\mathcal{N}}(\nu_{ul})$. In the case of complete redistribution through incoherent scattering in the presence of continuous opacity, the radiation phase space density evolves as

$$\dot{\hat{\mathcal{N}}} = \dot{\hat{\mathcal{N}}}_{\text{Hubble}} + \dot{\hat{\mathcal{N}}}_{\text{cont}} + \dot{\hat{\mathcal{N}}}_{\text{inc}}. \quad (36)$$

(We assume that the linewidth is small compared to ν_{ul} so that factors of ν/ν_{ul} appearing in the transport equation can be dropped.) In this section, we will develop each of these terms and solve the transport equations for the radiation profile over the line and the escape probability. Of these terms, the Hubble redshifting term is

$$\dot{\mathcal{N}}_{\text{Hubble}} = H\nu_{ul} \frac{\partial \mathcal{N}}{\partial \nu}. \quad (37)$$

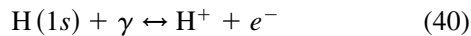
We will work in the steady-state approximation, where $\dot{\mathcal{N}} = 0$; possible corrections to this are considered in Paper II. Then, frequency provides a convenient domain over which to solve for \mathcal{N} , moving the Hubble term and dividing by $H\nu_{ul}$. Breaking up $\dot{\mathcal{N}}_{\text{cont}}$ and $\dot{\mathcal{N}}_{\text{inc}}$ into emission and absorption pieces, there are four terms that appear in the steady-state equation for the phase space density: absorption and emission by continuum processes and emission and absorption by incoherent processes in the line. We may write these as

$$\frac{\partial \mathcal{N}}{\partial \nu} = \left(\frac{\partial \mathcal{N}}{\partial \nu} \right)_{\text{cont-abs}} + \left(\frac{\partial \mathcal{N}}{\partial \nu} \right)_{\text{inc-abs}} + \left(\frac{\partial \mathcal{N}}{\partial \nu} \right)_{\text{cont-em}} + \left(\frac{\partial \mathcal{N}}{\partial \nu} \right)_{\text{inc-em}}. \quad (38)$$

The continuum absorption term has already been determined (Eq. (27)) and is $\eta_c \mathcal{N}(\nu)$. The line absorption term depends on the line profile and is $\tau_S \phi(\nu) \mathcal{N}(\nu)$ since $\tau_S \phi(\nu)$ is the optical depth per unit frequency. The continuum emission term is

$$\left(\frac{\partial \mathcal{N}}{\partial \nu} \right)_{\text{cont-em}} = -\eta_c \mathcal{N}_C, \quad (39)$$

where \mathcal{N}_C is the phase space density of photons that would be required for the reaction



to be in equilibrium. The usual equilibrium constant argument shows that $\mathcal{N}_C \propto n_{\text{HII}} n_e / n_{\text{HI}}$; the proportionality constant can be determined from the principle of detailed balance as

$$\mathcal{N}_C(\nu) = \left(\frac{n_e n_c}{n_i} \right) \left(\frac{n_i}{n_e n_c} \right)^{\text{LTE}} e^{-h\nu/k_B T_m}. \quad (41)$$

Since we have seen that hydrogen is in Saha equilibrium during the relevant era, and that $T_m = T_r$, we have $\mathcal{N}_C(\nu) = e^{-h\nu/k_B T_r}$. The He I] $n^3 P^o - 1^1 S$ and [He I] $n^1 D - 1^1 S$ lines are at very high energies (≥ 20.6 eV), so the photon phase space density $\mathcal{N} \ll 1$ and we can neglect stimulated emission and other consequences of the photon's bosonic nature. The line emission term is

$$\left(\frac{\partial \mathcal{N}}{\partial \nu} \right)_{\text{inc-em}} = -\tau_S \phi(\nu) \mathcal{N}_L, \quad (42)$$

where \mathcal{N}_L is the phase space density that would exist if

only the line processes were important. This can also be determined by setting the excitation rate $x_l(g_u/g_l)A_{u \rightarrow l} \mathcal{N}_L$ equal to the deexcitation rate $x_u A_{u \rightarrow l}(1 + \mathcal{N}_L)$:

$$\mathcal{N}_L = \frac{x_u}{x_l(g_u/g_l) - x_u}. \quad (43)$$

The transport equation is thus

$$\frac{\partial \mathcal{N}}{\partial \nu} = \eta_c (\mathcal{N} - \mathcal{N}_C) + \tau_S \phi(\nu) (\mathcal{N} - \mathcal{N}_L). \quad (44)$$

It has the general solution:

$$\mathcal{N}(\nu) = e^{\Phi_1(\nu)} \left\{ C - \int_{\nu_2}^{\nu} [\mathcal{N}_C \eta_c + \mathcal{N}_L \tau_S \phi(\tilde{\nu})] e^{-\Phi_1(\tilde{\nu})} d\tilde{\nu} \right\}, \quad (45)$$

where

$$\Phi_1(\nu) = \int_{\nu_1}^{\nu} [\eta_c + \tau_S \phi(\tilde{\nu})] d\tilde{\nu}. \quad (46)$$

Here ν_1 is an arbitrary but fixed frequency, and ν_2 is the frequency at which we set the initial condition. It is convenient to expand Eq. (45) into the pieces that depend linearly on the constant C and on \mathcal{N}_C and \mathcal{N}_L :

$$\mathcal{N}(\nu) = C I_i(\nu) + \mathcal{N}_C I_C(\nu) + \mathcal{N}_L I_L(\nu), \quad (47)$$

where the individual profiles are

$$\begin{aligned} I_i(\nu) &= e^{\Phi_1(\nu)}, \\ I_C(\nu) &= -e^{\Phi_1(\nu)} \int_{\nu_2}^{\nu} \eta_c e^{-\Phi_1(\tilde{\nu})} d\tilde{\nu}, \quad \text{and} \\ I_L(\nu) &= -e^{\Phi_1(\nu)} \int_{\nu_2}^{\nu} \tau_S \phi(\tilde{\nu}) e^{-\Phi_1(\tilde{\nu})} d\tilde{\nu}. \end{aligned} \quad (48)$$

We integrate this phase space density over the profile, and break the integral into three pieces that emphasize the physical processes:

$$\bar{\mathcal{N}} = C \bar{I}_i + \mathcal{N}_C \bar{I}_C + \mathcal{N}_L \bar{I}_L. \quad (49)$$

Here the overbar denotes averaging over the line profile, e.g.

$$\bar{\mathcal{N}} = \int_{-\infty}^{\infty} \phi(\nu) \mathcal{N}(\nu) d\nu. \quad (50)$$

Bringing the outer exponent under the integral in the expression of \bar{I}_L :

$$\begin{aligned} \bar{I}_L &= - \int_{-\infty}^{\infty} \phi(\nu) \int_{\nu_2}^{\nu} \tau_S \phi(\tilde{\nu}) \exp \left\{ - \int_{\nu}^{\tilde{\nu}} [\eta_c \right. \\ &\quad \left. + \tau_S \phi(y)] dy \right\} d\tilde{\nu} d\nu. \end{aligned} \quad (51)$$

We will take the starting frequency to be on the far blue side of the line ($\nu_2 \rightarrow \infty$), appropriate for expanding media

[73]. With this choice, it is convenient to switch the order of integration and absorb the leading minus sign. The \bar{I}_L line integral is related to the original Sobolev problem by setting $\eta_c = 0$,

$$\bar{I}_L|_{\eta_c=0} = 1 - \frac{1 - e^{-\tau_S}}{\tau_S} = 1 - P_S. \quad (52)$$

Simply, $P_S = 1 - \bar{I}_L(\eta_c = 0)$. We follow Rybicki and Hummer [72] in then calculating the difference in the line integral with and without continuum absorption (which is related to the probability of absorption between incoherent scattering events, P_C):

$$\begin{aligned} \Delta\bar{I}_L &= \bar{I}_L - \bar{I}_L|_{\eta_c=0} \\ &= - \int_{-\infty}^{\infty} \phi(\nu) \int_{\nu_2}^{\nu} \tau_S \phi(\tilde{\nu}) \exp\left[-\tau_S \int_{\nu}^{\tilde{\nu}} \phi(y) dy\right] \\ &\quad \times [e^{-\eta_c(\tilde{\nu}-\nu)} - 1] d\tilde{\nu} d\nu. \end{aligned} \quad (53)$$

We integrate this numerically over a Voigt profile to find the probability of absorption by a continuum process. The Voigt profile and its integral have a wide dynamic range—details of evaluating the integral are described in Appendix B. The main goal is to find the integral of the radiation phase space density over the line profile ($\bar{\mathcal{N}}$ in Eq. (49)), and the modified escape probability. Examples of line radiation profiles with incoherent scattering and continuum opacity are shown in Fig. 8.

The overall value of $\bar{\mathcal{N}}$ is required in order to compute excitation and deexcitation rates. With the boundary $\nu_2 \rightarrow \infty$, we have $\Phi_1(\nu_2) \rightarrow \infty$ and hence $C \rightarrow 0$, while \bar{I}_i re-

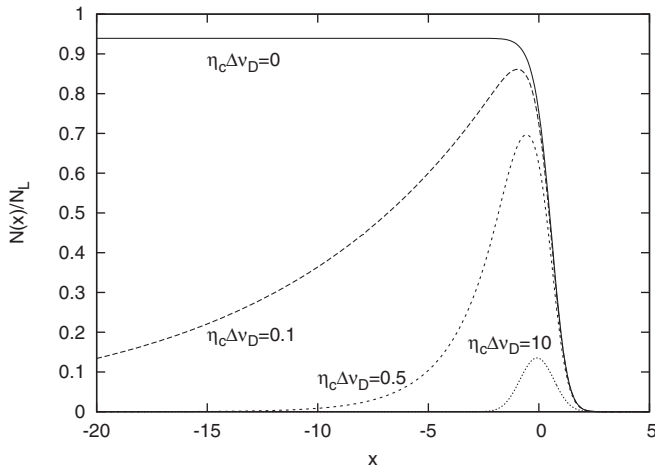


FIG. 8. The radiation profile near the intercombination line $1^1S_0 \rightarrow 2^3P_1^o$ resonance with Voigt parameter $a = \Gamma_{\text{line}}/(4\pi\Delta\nu_D) = 10^{-5}$ for the Sobolev optical depth $\tau_S = 2.8$ and $\mathcal{N}_C = 0$, for several sample continuum optical depths $\eta_c\Delta\nu_D$, showing the effect of continuum opacity. Because of the low optical depth and small natural linewidth, very little radiation extends more than three doppler widths above the line, and the effect of the continuum is significant in relaxing the radiation phase space density near line center.

mains finite at fixed ν_1 . Therefore

$$\bar{\mathcal{N}} = \mathcal{N}_C \bar{I}_C + \mathcal{N}_L \bar{I}_L. \quad (54)$$

Now, if we had $\mathcal{N}_C = \mathcal{N}_L$, the solution to Eq. (44) would be simply $\mathcal{N} = \mathcal{N}_L$ and hence $\bar{\mathcal{N}} = \mathcal{N}_L$. Thus $\bar{I}_C + \bar{I}_L = 1$ and hence

$$\begin{aligned} \bar{\mathcal{N}} &= \mathcal{N}_C \bar{I}_C + \mathcal{N}_L (1 - P_S + \Delta\bar{I}_L) \\ &= \mathcal{N}_C (P_S - \Delta\bar{I}_L) + \mathcal{N}_L (1 - P_S + \Delta\bar{I}_L). \end{aligned} \quad (55)$$

The net downward transition rate from u to l is

$$\dot{x}|_{\text{line}} = A_{u \rightarrow l} \left[x_u (1 + \bar{\mathcal{N}}) - \frac{g_u}{g_l} x_l \bar{\mathcal{N}} \right]. \quad (56)$$

For $x_u \ll x_l$ and $\bar{\mathcal{N}} \ll 1$, this can be reexpressed in terms of \mathcal{N}_L as

$$\dot{x}|_{\text{line}} = A_{u \rightarrow l} \frac{g_u}{g_l} x_l (\mathcal{N}_L - \bar{\mathcal{N}}), \quad (57)$$

from which we find

$$\begin{aligned} \dot{x}|_{\text{line}} &= A_{u \rightarrow l} \frac{g_u}{g_l} x_l (P_S - \Delta\bar{I}_L) (\mathcal{N}_L - \mathcal{N}_C) \\ &= P_{\text{esc}} A_{u \rightarrow l} \left(x_u - \frac{g_u}{g_l} x_l \mathcal{N}_C \right), \end{aligned} \quad (58)$$

where $P_{\text{esc}} = P_S - \Delta\bar{I}_L$. Note that $\Delta\bar{I}_L$ is manifestly negative according to Eq. (53), so continuum opacity enhances the escape probability. The transition rate from level u to l is then set by the occupations of the states, and by the radiative escape probability, P_{esc} .

Before continuing, we note one subtlety of our analysis. We have assumed that the continuum on the blue side of the line is optically thick to H I photoionization, or equivalently, we neglected feedback from unabsorbed spectral distortions from a higher-frequency line. [Formally this was done when we argued that $\Phi_1(\nu_2) \rightarrow \infty$.] This is not as restrictive an assumption as it seems (even though it is violated at the beginning of He I recombination), because the widths of the He I lines are small compared to their separation. Thus if the continuum opacity *within* a line can be neglected, in which case we know that the correct escape probability is the Sobolev result, $P_{\text{esc}} = P_S$ (and the converse, where opacity is important within the line only once with transport of the distortion between lines is suppressed). Since our solution here for P_{esc} reduces to the Sobolev optical depth in the limit where continuum opacity within the line is turned off, it follows that using this P_{esc} in the level code in the form

$$\dot{x}|_{\text{line}} = P_{\text{esc}} A_{u \rightarrow l} \left(x_u - \frac{g_u}{g_l} x_l \mathcal{N}_+ \right), \quad (59)$$

i.e. replacing \mathcal{N}_C in Eq. (58) with \mathcal{N}_+ , will recover the correct solution in both the case where continuum opacity

within the line is important (where we have $\mathcal{N}_+ = \mathcal{N}_C$) and the case where it is not.

The total escape probability is too time consuming to calculate on a case-by-case basis, as part of the level code. Instead, we calculate a lookup table of modified escape probabilities as a function of the He I ground state fraction and redshift, assuming that the neutral hydrogen population is in Saha equilibrium during He I recombination. The details of this calculation are given in Appendix B. The Monte Carlo methods developed in Sec. VD also generate a grid of modified escape probabilities as a function of redshift and the occupation of the He I ground state. These are log-interpolated and applied in to the recombination level code, as described in Sec. VE.

V. THE MODIFIED ESCAPE PROBABILITY INCLUDING COHERENT SCATTERING

In the previous section, we considered the problem of calculating the decay rate of He I lines with no coherent scattering. This section aims to include coherent scattering in the problem, which is necessary in order to handle the Lyman-like series of lines, He I $n^1P^o - 1^1S$. Coherent scattering complicates the problem because the frequency distribution of photons emitted in the line depends on the existing spectrum of radiation (photons are not completely redistributed across the line). Our approach to this problem will be to realize that a helium atom reaches the upper level $n^1P^o_1$ by emitting or absorbing a photon, and then it leaves this level by emitting or absorbing a photon. Therefore, all processes involving this level can be regarded as a form of resonant two-photon absorption, resonant two-photon emission, resonant Raman scattering, and resonant Rayleigh scattering. Physically one should write down the rates for these processes and solve the relevant level population/radiative transfer problem.

A. Setup

The goal here is to replace the usual treatment of the line through one-photon processes by an inherently two-photon treatment (two-photon absorption, two-photon emission, and scattering) in which u represents the intermediate state. In the case of each He I $n^1P^o - 1^1S$ line, we will denote the lower level by $l = 1^1S$ and the upper level by $u = n^1P^o$. The rates for two-photon processes in the vicinity of resonance can be expressed in terms of the constituent one-photon absorption and emission processes, and depend, in particular, on the branching fractions that determine the fate of a helium atom in level u . Throughout, we will make several assumptions about the radiation field and rates during recombination:

- (1) $\mathcal{N}(\nu_{ul}) \ll 1$ implies that stimulated emission in He I $n^1P^o - 1^1S$ lines can be neglected. (This is because $h\nu_{ul} \gg k_B T_r$ so the Wien curve has $\mathcal{N} \ll 1$, and the spectral distortion raises \mathcal{N} to at most $\sim x_{n^1P^o}/3x_{1^1S} \ll 1$.)

- (2) The transitions from u to other excited states (or the continuum) see approximately a blackbody spectrum and are Sobolev optically thin.
- (3) The time for x_u to change significantly is much longer than the lifetime of the state, so we can work in a ‘‘steady state.’’

An atom in level u has three possible fates. It could decay to the ground level l with the rate $A_{u \rightarrow l}$ (we neglect stimulated emission in the $2^1P^o - 1^1S$ line under assumption 1). It may also decay to another level a with lower energy $E_a < E_u$, with rate $A_{u \rightarrow a}[1 + \mathcal{N}(\nu_{ua})]$. A third possibility is that an atom in level u could absorb a photon and transit to an even higher level b with rate $A_{b \rightarrow u}(g_b/g_u)\mathcal{N}(\nu_{bu})$. (Note that b could be a continuum level.) The overall width of the level u is then

$$\Gamma_u = A_{u \rightarrow l} + \sum_{a < u, a \neq l} A_{u \rightarrow a}[1 + \mathcal{N}(\nu_{ua})] + \sum_{b > u} A_{b \rightarrow u} \frac{g_b}{g_u} \mathcal{N}(\nu_{bu}). \quad (60)$$

(Note that the summation over b includes an implied integration over continuum states.) It is convenient to define the rates

$$R_{ui} = \begin{cases} A_{u \rightarrow i}[1 + \mathcal{N}(\nu_{ui})] & E_i < E_u \\ A_{i \rightarrow u}(g_i/g_u)\mathcal{N}(\nu_{iu}) & E_i > E_u \end{cases} \quad (61)$$

so that $\Gamma_u = A_{u \rightarrow l} + \sum_i R_{ui, i \neq l}$. The fractional contribution to this width from a final level will be denoted $f_i = R_{ui}/\Gamma_u$, where we identify $R_{ul} = A_{u \rightarrow l}$. This should be interpreted as the probability that u will transit to i , given all of its options. The radiative rate for one-photon radiative transitions from some level $i \neq l$ to u is

$$R_{iu} = \begin{cases} A_{u \rightarrow i}(g_u/g_i)\mathcal{N}(\nu_{ui}) & E_i < E_u \\ A_{i \rightarrow u}[1 + \mathcal{N}(\nu_{iu})] & E_i > E_u \end{cases}. \quad (62)$$

The radiative rate for one-photon excitation from l to u is similar, except that one must average the photon phase space density over the line profile because the phase space density may be strongly frequency dependent (unlike the $u \leftrightarrow e$ transitions where one is dealing with a blackbody radiation field):

$$R_{lu} = A_{u \rightarrow l} \frac{g_u}{g_l} \bar{\mathcal{N}}. \quad (63)$$

Figure 9 summarizes the rates R_{lu} , R_{lu} , R_{lu} , and R_{lu} for the lower excitation states of helium.

It is straightforward to write down the net rate of production (or destruction) of each level via two-photon processes involving the excited state u , in terms of the rates (Eqs. (60)–(63)). It is simply the difference of destruction rate of level i via transition to u , and the rate of production of i from all modes involving u :

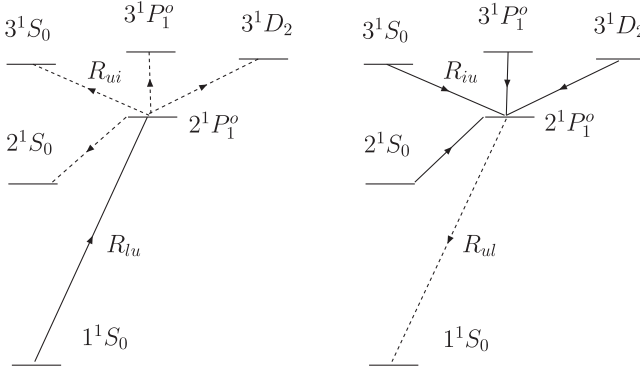


FIG. 9. The transition $2^1P_1^o - 1^1S$ interpreted as a two-photon process with $2^1P_1^o$ as an intermediate resonant state. In an incoherent scattering through He I $1^1S_0 \leftrightarrow 2^1P_1^o$, the incoming photon excites $1^1S_0 \rightarrow 2^1P_1^o$. The atom absorbs a second photon and explores several intermediate states before decaying through $2^1P_1^o - 1^1S$, emitting a $2^1P_1^o - 1^1S$ photon with complete redistribution. In coherent scattering, only 1^1S_0 and $2^1P_1^o$ are involved, and the outgoing photon is emitted with the same energy as the incoming photon in the rest frame of the atom.

$$\begin{aligned} \dot{x}_i|_u &= -R_{iu}x_i + \sum_{j \neq u} x_j R_{ju} f_i \\ &= -R_{iu}x_i + R_{ui} \Gamma_u^{-1} \sum_{j \neq u} x_j R_{ju}. \end{aligned} \quad (64)$$

If we knew exactly the rate coefficients R_{ul} and R_{lu} , Eq. (64) would be easy to incorporate into the level codes. That is because we can simply write the steady-state population of u as its production rate multiplied by its lifetime Γ_u^{-1} ,

$$x_u = \Gamma_u^{-1} \sum_{j \neq u} x_j R_{ju}. \quad (65)$$

Then for $i \neq l, u$, Eq. (64) is exactly equivalent to the standard rate equation (Eq. (8)).

The rate equation for the ground level is modified to become

$$\dot{x}_l|_u = -R_{lu}x_l + R_{ul}x_u, \quad (66)$$

and that for u becomes

$$0 = -\sum_{i \neq u} R_{ui}x_u + \sum_{i \neq u} R_{iu}x_i. \quad (67)$$

These two are also similar to Eq. (8) except that the left-hand side of Eq. (67) is zero, as appropriate for a steady-state solution, and the rates R_{ul} and R_{lu} may differ from the Sobolev values. Indeed, the *only* modification needed in the level code is that these rates need to be replaced with the values $A_{u \rightarrow i}$ and Eq. (63). The only nontrivial part of the calculation is to compute $\bar{\mathcal{N}}$ appearing in Eq. (63). The calculation of $\bar{\mathcal{N}}$ will occupy the rest of this section.

In some parts of this section we will define the additional branching fractions $f_{\text{coh}} \equiv f_l$ and $f_{\text{inc}} \equiv 1 - f_l$. These

represent the branching fractions for absorption of a line photon to result in coherent scattering (f_{coh}) or incoherent scattering (f_{inc}). We also use the portions of the Sobolev optical depth due to these processes, $\tau_{\text{coh}} \equiv \tau_S f_l$ and $\tau_{\text{inc}} \equiv \tau_S (1 - f_l)$.

B. The equation of radiative transfer

In order to compute $\bar{\mathcal{N}}$, we need to construct and solve the radiative transfer equation for the photon phase space density in the vicinity of the line, $\mathcal{N}(\nu)$. The line profile evolves according to four effects: the Hubble redshifting of the photons; absorption and emission in the H I continuum; coherent scattering; and incoherent emission/absorption processes (i.e. resonant Raman scattering and two-photon emission/absorption, whose line profiles do not depend on the incident radiation field). Schematically, we write

$$\dot{\mathcal{N}} = \dot{\mathcal{N}}_{\text{Hubble}} + \dot{\mathcal{N}}_{\text{cont}} + \dot{\mathcal{N}}_{\text{coh}} + \dot{\mathcal{N}}_{\text{inc}}. \quad (68)$$

The continuum contribution was solved in Sec. IV:

$$\dot{\mathcal{N}}_{\text{cont}} = -H\nu_{ul}\eta_c(\mathcal{N} - \mathcal{N}_C). \quad (69)$$

A photon has a probability per unit time of undergoing a coherent scatter given by $H\nu_{ul}\tau_{\text{coh}}\phi(\nu)$, where $\tau_{\text{coh}} = \tau_S f_l$, the Sobolev optical depth to any type of absorption times f_l , where f_l is the fraction of photon absorptions that are followed directly by emission, $\phi(\nu)$ is the line profile in units of fraction of the integrated profile traversed per unit time (s^{-1}), and $H\nu_{ul}$ converts this to the fraction of the integrated profile traversed per unit frequency (Hz^{-1}). Thus we have

$$\begin{aligned} \dot{\mathcal{N}}_{\text{coh}}(\nu) &= -H\nu_{ul}\tau_{\text{coh}}\phi(\nu)\mathcal{N}(\nu) \\ &\quad + H\nu_{ul}\tau_{\text{coh}} \int \phi(\nu')\mathcal{N}(\nu')p(\nu|\nu')d\nu'. \end{aligned} \quad (70)$$

Here $p(\nu|\nu')$ is the probability distribution for the outgoing frequency ν of a coherently scattered photon conditioned on its ingoing frequency ν' . (This is commonly known as a redistribution function, and the relevant case here is of the R_{II} type [74].) It satisfies $\int p(\nu|\nu')d\nu = 1$.

Finally we come to incoherent processes, $\dot{\mathcal{N}}_{\text{inc}}$. The probability per unit time of incoherent scattering (i.e. excitation of an atom to u followed by transit to a state other than l) is $H\nu_{ul}\tau_{\text{inc}}\phi(\nu)$. The rate of incoherent emission processes (two-photon emission or resonant Raman scattering, $i \rightarrow u \rightarrow l$, with $i \neq l$) per H nucleus per unit time is $\sum_i x_i R_{iu} f_i$. Thus we have

$$\begin{aligned} \dot{\mathcal{N}}_{\text{inc}}(\nu) &= -H\nu_{ul}\tau_{\text{inc}}\phi(\nu)\mathcal{N}(\nu) \\ &\quad + \frac{n_{\text{H}}c^3}{8\pi\nu_{ul}^2} \sum_{i \neq l} x_i R_{iu} f_i \phi(\nu). \end{aligned} \quad (71)$$

(Here $n_{\text{H}}c^3/8\pi\nu_{ul}^2$ is a conversion factor: it is the number of H nuclei in a volume containing one photon mode per

unit frequency at ν_{ul} .) We note that $f_l = A_{u \rightarrow l}/\Gamma_u$, and using $x_u \ll x_l$, we may write

$$\begin{aligned} \frac{n_{\text{H}}c^3}{8\pi\nu_{ul}^2}f_l &= \frac{n_{\text{H}}c^3A_{u \rightarrow l}}{8\pi\nu_{ul}^2}\Gamma_u^{-1} = \frac{H\nu_{ul}\tau_S}{x_l(g_u/g_l) - x_u}\Gamma_u^{-1} \\ &\approx \frac{H\nu_{ul}g_l\tau_S}{g_u x_l \Gamma_u}. \end{aligned} \quad (72)$$

This turns Eq. (71) into

$$\dot{\mathcal{N}}_{\text{inc}}(\nu) = H\nu_{ul}\tau_{\text{inc}}\phi(\nu)[\mathcal{N}_{\text{L}}^{(0)} - \mathcal{N}(\nu)], \quad (73)$$

where we have defined

$$\mathcal{N}_{\text{L}}^{(0)} = \frac{g_l}{g_u x_l \Gamma_u f_{\text{inc}}} \sum_{i \neq l} x_i R_{iu}. \quad (74)$$

Note that $\mathcal{N}_{\text{L}}^{(0)}$ is not necessarily equal to the phase space density of photons in equilibrium with the line, which would be $\mathcal{N}_{\text{L}} = g_l x_u / g_u x_l$ for $x_u \ll x_l$. However, the two are related.

In steady state one may combine Eqs. (37), (69), (70), and (73) and set $\dot{\mathcal{N}} \rightarrow 0$ to yield

$$\begin{aligned} \frac{\partial \mathcal{N}}{\partial \nu} &= \eta_{\text{c}}[\mathcal{N}(\nu) - \mathcal{N}_{\text{C}}] + \tau_{\text{coh}} \left[\phi(\nu)\mathcal{N}(\nu) \right. \\ &\quad \left. - \int \phi(\nu')\mathcal{N}(\nu')p(\nu|\nu')d\nu' \right] \\ &\quad + \tau_{\text{inc}}\phi(\nu)[\mathcal{N}(\nu) - \mathcal{N}_{\text{L}}^{(0)}]. \end{aligned} \quad (75)$$

The parameters \mathcal{N}_{C} and $\mathcal{N}_{\text{L}}^{(0)}$ may be eliminated from this equation via the introduction of the variable

$$\xi(\nu) = \frac{\mathcal{N}(\nu) - \mathcal{N}_{\text{C}}}{\mathcal{N}_{\text{L}}^{(0)} - \mathcal{N}_{\text{C}}}, \quad (76)$$

or

$$\mathcal{N}(\nu) = \mathcal{N}_{\text{C}} + (\mathcal{N}_{\text{L}}^{(0)} - \mathcal{N}_{\text{C}})\xi(\nu). \quad (77)$$

Expressing Eq. (75) in terms of $\xi(\nu)$, we find

$$\begin{aligned} \frac{d}{d\nu}\xi(\nu) &= \tau_{\text{coh}} \left[\phi(\nu)\xi(\nu) - \int \phi(\nu')\xi(\nu')p(\nu|\nu')d\nu' \right] \\ &\quad + \eta_{\text{c}}\xi(\nu) + \tau_{\text{inc}}\phi(\nu)[\xi(\nu) - 1]. \end{aligned} \quad (78)$$

The boundary condition is that due to formally infinite continuum optical depth if we integrate to $\nu = +\infty$, we have $\xi_+ = 0$ (where again ξ_+ is the value of ξ on the blue side of the line). This may fail if the optical depth between lines τ_{LL} is not much larger than 1; the correction for this is discussed at the end of Sec. V C.

We will concern ourselves with solving Eq. (78) in Sec. V D using a Monte Carlo method. However before we do this we will investigate the implications of the solution by relating the value of $\xi(\nu)$ averaged across the line,

$$\bar{\xi} \equiv \int \xi(\nu)\phi(\nu)d\nu, \quad (79)$$

to the value of $\mathcal{N}_{\text{L}}^{(0)}$ and to the net decay rate $\dot{x}_l|_u$, which is the quantity we need to know in order to solve helium recombination.

C. Relation of $\mathcal{N}_{\text{L}}^{(0)}$ and $\bar{\xi}$ to decay rate

The objective of this section is to determine the rate $\dot{x}_l|_u$ in terms of quantities such as x_l , x_u , and f_l that can be computed easily in the level code, and the quantity $\bar{\xi}$ that emerges from the solution to Eq. (78).

As noted at the end of Sec. V A, the upward and downward transition rates in the $l \leftrightarrow u$ line are $R_{lu} = (g_u/g_l)A_{u \rightarrow l}\bar{\mathcal{N}}$ and $R_{ul} = A_{u \rightarrow l}$, respectively. Averaging Eq. (77) over the line profile, we find that

$$R_{lu} = \frac{g_u}{g_l}A_{u \rightarrow l}[\mathcal{N}_{\text{C}} + (\mathcal{N}_{\text{L}}^{(0)} - \mathcal{N}_{\text{C}})\bar{\xi}]. \quad (80)$$

It follows from Eq. (65) that

$$x_u = \Gamma_u^{-1} \left\{ \sum_{i \neq l, u} x_i R_{iu} + \frac{g_u}{g_l} x_l A_{u \rightarrow l} [\mathcal{N}_{\text{C}} + (\mathcal{N}_{\text{L}}^{(0)} - \mathcal{N}_{\text{C}})\bar{\xi}] \right\}. \quad (81)$$

The term $\sum_{i \neq l, u} x_i R_{iu}$ also appears in Eq. (74), so we can replace it with $\mathcal{N}_{\text{L}}^{(0)}$. Noting also that $A_{u \rightarrow l}/\Gamma_u = f_l = f_{\text{coh}}$, we may write

$$x_u = \frac{g_u x_l}{g_l} \{ f_{\text{inc}} \mathcal{N}_{\text{L}}^{(0)} + f_{\text{coh}} [\mathcal{N}_{\text{C}} + (\mathcal{N}_{\text{L}}^{(0)} - \mathcal{N}_{\text{C}})\bar{\xi}] \}. \quad (82)$$

The quantity in braces is $\mathcal{N}_{\text{L}} = g_l x_u / g_u x_l$, i.e. the phase space density of photons that would be in equilibrium with the l and u level populations (again assuming $x_u \ll x_l$):

$$\mathcal{N}_{\text{L}} = f_{\text{inc}} \mathcal{N}_{\text{L}}^{(0)} + f_{\text{coh}} [\mathcal{N}_{\text{C}} + (\mathcal{N}_{\text{L}}^{(0)} - \mathcal{N}_{\text{C}})\bar{\xi}]. \quad (83)$$

If, however, x_l and x_u are known (they are directly available in the level code), we may rearrange this equation to solve for $\mathcal{N}_{\text{L}}^{(0)}$ in terms of \mathcal{N}_{L} , \mathcal{N}_{C} , f_{coh} , and $\bar{\xi}$. After some algebra, we find

$$\mathcal{N}_{\text{L}}^{(0)} = \frac{\mathcal{N}_{\text{L}} - f_{\text{coh}}(1 - \bar{\xi})\mathcal{N}_{\text{C}}}{1 - f_{\text{coh}}(1 - \bar{\xi})}. \quad (84)$$

In order to determine the upward transition rate, we need to calculate $\bar{\mathcal{N}}$, which is

$$\begin{aligned} \bar{\mathcal{N}} &= \mathcal{N}_{\text{C}} + (\mathcal{N}_{\text{L}}^{(0)} - \mathcal{N}_{\text{C}})\bar{\xi} \\ &= \mathcal{N}_{\text{C}} + \frac{(\mathcal{N}_{\text{L}} - \mathcal{N}_{\text{C}})\bar{\xi}}{1 - f_{\text{coh}}(1 - \bar{\xi})}. \end{aligned} \quad (85)$$

Then we have

$$\begin{aligned} \dot{x}_l|_u &= -R_{lu}x_l + R_{ul}x_u = A_{u \rightarrow l} \left(-\frac{g_u}{g_l} x_l \bar{\mathcal{N}} + x_u \right) \\ &= \frac{g_u}{g_l} A_{u \rightarrow l} x_l (-\bar{\mathcal{N}} + \mathcal{N}_{\text{L}}). \end{aligned} \quad (86)$$

One can eliminate $\bar{\mathcal{N}}$ using Eq. (85), and algebraic simplification then yields

$$\dot{x}_l|_u = \frac{g_u}{g_l} A_{u \rightarrow l} x_l (\mathcal{N}_L - \mathcal{N}_C) \left(1 - \frac{\bar{\xi}}{1 - f_{\text{coh}}(1 - \bar{\xi})} \right). \quad (87)$$

We now recall that \mathcal{N}_C is very nearly equal to the black-body function since hydrogen is in Saha equilibrium during He I recombination.

$$\dot{x}_l|_u = A_{u \rightarrow l} \left(x_u - \frac{g_u}{g_l} x_l \mathcal{N}_C \right) P_{\text{esc}}, \quad (88)$$

where

$$P_{\text{esc}} = 1 - \frac{\bar{\xi}}{1 - f_{\text{coh}}(1 - \bar{\xi})} = \frac{(1 - \bar{\xi})f_{\text{inc}}}{1 - f_{\text{coh}}(1 - \bar{\xi})}. \quad (89)$$

Before continuing, we wish to generalize this equation to remove one assumption we have made about continuum opacity. Recall that we have assumed a finite continuum optical depth per unit frequency, which when integrated to $\nu \rightarrow +\infty$ gives formally infinite optical depth and hence drives \mathcal{N}_+ to its equilibrium value. In practice there are times early in helium recombination where the continuum opacity within a line is unimportant, and the continuum optical depth between the line of interest and the next higher-frequency line is not $\gg 1$. In these cases \mathcal{N}_+ may differ from \mathcal{N}_{pl} due to feedback. We may trivially correct for this by noting that if feedback is important then the line-line optical depth τ_{LL} is of order 1 or less. In this case, then the continuum opacity within an individual He I line is negligible, so in Eq. (75) we have $\eta_c \approx 0$. In this case, we are free to replace \mathcal{N}_C in Eq. (75) with \mathcal{N}_+ without consequence. Making this replacement in the subsequent equations, in particular, Eq. (76), we find that ξ on the blue side of the line is zero since $\mathcal{N} = \mathcal{N}_+$ there. Hence the boundary condition $\xi_+ = 0$ that we were using earlier applies, and Eq. (88) is also valid, except that we need to replace $\mathcal{N}_C \rightarrow \mathcal{N}_+$:

$$\dot{x}_l|_u = A_{u \rightarrow l} \left(x_u - \frac{g_u}{g_l} x_l \mathcal{N}_+ \right) P_{\text{esc}}. \quad (90)$$

This equation is very similar to the Sobolev rate, Eq. (8). The only difference (aside from the factor of $1 + \mathcal{N}_+$, which is irrelevant since $\mathcal{N}_+ \ll 1$ for these lines) is the Sobolev escape probability has been replaced with P_{esc} , the escape probability including partial redistribution.

D. Monte Carlo method: theory

So far in this section, we have constructed an equation of radiative transfer (Eq. (78)) for the He I $n^1P^o - 1^1S$ lines, and related the effective line escape probability to its solution (Eq. (89)). There is only one major step left: to solve Eq. (78) for the full partial redistribution plus continuous opacity problem.

A variety of approaches have been taken in the literature for solving line radiative transfer equations including co-

herent scattering terms. One approach is the diffusive, Fokker-Planck approximation [73] which replaces the redistribution integral (Eq. (70)) with a second-order differential operator. This results in a second-order ordinary differential equation (ODE) instead of integro-differential equation, which is a substantial improvement for most numerical techniques. The other possibilities are the conversion of the equation of radiative transfer into a linear algebra problem or a solution through Monte Carlo methods [75–81]. The latter two have the advantage of being usable in the Doppler core of the lines, which we expect to be important since for e.g. He I $2^1P^o - 1^1S$ lines, the width of the line that is optically thick to incoherent processes $\Delta\nu_{\text{line}}$ is only $\sim 30\Delta\nu_{\text{D}}$ during most of He I recombination. Therefore we have not used the Fokker-Planck approach, which we believe is better suited for studying the far damping wings of very optically thick lines such as H I Ly α . (The Fokker-Planck operator assumes that many scattering events transport a photon over a region where the line shape varies slowly; yet in the core of the line, single scatterings can transport a photon over the width of the core.) We have chosen the Monte Carlo approach here, mainly because we had a preexisting code that was capable of handling the problem with minor modifications [75].

The basic plan of the Monte Carlo simulation is as follows: we begin by injecting a photon with frequency distribution drawn from the Voigt line profile, $\phi(\nu)$. We simulate its fate by assuming that it redshifts at the rate $\dot{\nu} = -H\nu_{ul}$; undergoes coherent scattering with probability per unit time $H\nu_{ul}\tau_S f_l \phi(\nu)$; undergoes continuum absorption with probability per unit time $H\nu_{ul}\eta_c$; and undergoes incoherent absorption with probability per unit time $H\nu_{ul}\tau_S(1 - f_l)\phi(\nu)$. The simulation is terminated if the photon is absorbed in the H I continuum, if it redshifts out of the line, or if it undergoes incoherent absorption in He I. Note that within the idealized conditions $\eta_c = \text{constant}$ of the simulation, a photon that redshifts out of the line will eventually be absorbed by the continuum so long as $\eta_c > 0$ (though in reality the photon would eventually reach other He I lines or redshift to below 13.6 eV). Therefore only the total probability of these two results is meaningful. We thus denote by P_{MC} the probability that a photon in the Monte Carlo simulation is terminated by redshifting out of the line or by continuum absorption, and let $1 - P_{\text{MC}}$ denote the probability that the photon is terminated by incoherent absorption. The implementation of the Monte Carlo simulation is described in Appendix C; the rest of this section will be devoted to the problem of extracting $\bar{\xi}$ from the Monte Carlo simulation. In particular, we will prove that $\bar{\xi} = 1 - P_{\text{MC}}$.

Our proof goes as follows. We begin by considering the probability distribution $\Pi(\nu)$ of the photon frequency in the Monte Carlo simulation at any specified time. [Note that this is not the same as the histogram of frequencies at which the photon scatters, which is $\propto \Pi(\nu)\phi(\nu)$ because

the scattering rate is proportional to $\phi(\nu)$.] Now from elementary considerations the probability distribution satisfies

$$\begin{aligned} \dot{\Pi}(\nu) = & H\nu_{ul} \left\{ \frac{\partial \Pi}{\partial \nu} - \eta_c \Pi(\nu) - \tau_{\text{inc}} \phi(\nu) \Pi(\nu) \right. \\ & \left. - \tau_{\text{coh}} \left[\phi(\nu) \Pi(\nu) - \int \phi(\nu') \Pi(\nu') p(\nu|\nu') d\nu' \right] \right\} \\ & + \Gamma_{\text{inj}} \phi(\nu), \end{aligned} \quad (91)$$

where Γ_{inj} is the rate of injection of photons in the Monte Carlo simulation. Then the steady-state distribution satisfies

$$\begin{aligned} \frac{\partial \Pi}{\partial \nu} = & \eta_c \Pi(\nu) + \tau_{\text{inc}} \phi(\nu) \Pi(\nu) + \tau_{\text{coh}} \left[\phi(\nu) \Pi(\nu) \right. \\ & \left. - \int \phi(\nu') \Pi(\nu') p(\nu|\nu') d\nu' \right] - \frac{\Gamma_{\text{inj}}}{H\nu_{ul}} \phi(\nu). \end{aligned} \quad (92)$$

This equation has a striking resemblance to Eq. (78). They are both linear inhomogeneous integro-differential equations, and they obey the same boundary condition, namely, that ξ and Π go to zero at high frequency (the photons are in equilibrium with H I on the blue side of the line). The only difference is in the source terms: the source term in Eq. (78) is $-\tau_{\text{inc}} \phi(\nu)$, whereas the source term in Eq. (92) is $-(\Gamma_{\text{inj}}/H\nu_{ul}) \phi(\nu)$. These source terms differ only by a constant scaling factor, and hence the solutions are scaled versions of each other with the same scaling factor:

$$\Pi(\nu) = \frac{\Gamma_{\text{inj}}}{H\nu_{ul}\tau_{\text{inc}}} \xi(\nu). \quad (93)$$

We now note that in the Monte Carlo method, photons are injected (the simulation is restarted with a new photon) when the photon is absorbed in either an incoherent process or by H I. Practically, the frequency span of the simulation is finite, yet photons that eventually redshift through the simulation boundaries will eventually be absorbed in a continuum event (assuming the opacity is nonzero). Therefore $\Gamma_{\text{inj}} = \Gamma_{\text{inc}} + \Gamma_{\text{cont}}$, where Γ_{inc} and Γ_{cont} are the rates of removal of photons by incoherent scattering and continuum absorption, respectively. Of these, Γ_{inc} is obtained by averaging the incoherent scattering rate $\tau_{\text{inc}} \phi(\nu)$ over the probability distribution, which yields

$$\Gamma_{\text{inc}} = H\nu_{ul}\tau_{\text{inc}}\bar{\Pi}. \quad (94)$$

[Here $\bar{\Pi}$ denotes averaging of $\Pi(\nu)$ over the line profile $\phi(\nu)$, which is equal to the average of the line profile over the photon probability distribution $\Pi(\nu)$.] The rate of removal via continuum opacity is simply

$$\Gamma_{\text{cont}} = H\nu_{ul}\eta_c. \quad (95)$$

Therefore we may write Eq. (93) as

$$\Pi(\nu) = \left(\bar{\Pi} + \frac{\eta_c}{\tau_{\text{inc}}} \right) \xi(\nu). \quad (96)$$

Multiplying both sides by $\phi(\nu)$ and integrating yields

$$\bar{\Pi} = \left(\bar{\Pi} + \frac{\eta_c}{\tau_{\text{inc}}} \right) \bar{\xi}, \quad (97)$$

from which we may find

$$\bar{\xi} = \frac{\bar{\Pi}}{\bar{\Pi} + \eta_c/\tau_{\text{inc}}}. \quad (98)$$

Now recalling Eqs. (94) and (95), we see that

$$\bar{\xi} = \frac{\Gamma_{\text{inc}}}{\Gamma_{\text{inc}} + \Gamma_{\text{cont}}} = \frac{\Gamma_{\text{inc}}}{\Gamma_{\text{inj}}} = 1 - \frac{\Gamma_{\text{cont}}}{\Gamma_{\text{inj}}} = 1 - P_{\text{MC}}. \quad (99)$$

This result connects the Monte Carlo method to the parameter $\bar{\xi}$ needed in the level code. Written directly in terms of P_{MC} , the modified escape probability (Eq. (90)) is

$$P_{\text{esc}} = \frac{P_{\text{MC}} f_{\text{inc}}}{1 - f_{\text{coh}} P_{\text{MC}}}. \quad (100)$$

Before continuing, we note several properties and limiting cases of Eq. (100). Since it is obvious that P_{MC} and f_{coh} , being probabilities, are in the range from 0 to 1, and we recall that $f_{\text{coh}} + f_{\text{inc}} = 1$, it is easily seen that P_{esc} is also in the range from 0 to 1 (hence its interpretation as an ‘‘escape probability’’). In the limit where there is no coherent scattering, we have, unsurprisingly, $P_{\text{esc}} = P_{\text{MC}}$: the effective escape probability P_{esc} appearing in the rate equations is exactly the probability of line escape or continuum absorption in the Monte Carlo simulation. In an optically thin line where essentially all photons in the Monte Carlo escape, $P_{\text{MC}} = 1$, then we find $P_{\text{esc}} = 1$. Finally, if $P_{\text{MC}} \ll 1$ so that almost all photons emitted in the line undergo incoherent reabsorption, we have $P_{\text{esc}} = P_{\text{MC}} f_{\text{inc}}$: the escape probability in the rate equations becomes the escape probability in the Monte Carlo simulation times the fraction of the Sobolev optical depth due to incoherent processes.

The Monte Carlo method described here raises two theoretical questions: first, does the escape probability in Eq. (100) coincide with that calculated in Sec. IV, as one would expect; and second, is the standard Sobolev result recovered in the absence of continuum absorption? In Appendix D, we show that the answer to the first question is in the affirmative. As for the second question, we find (also in Appendix D) that by setting $\eta_c = 0$ the standard Sobolev escape probability is recovered *if* the line is sufficiently optically thick, i.e. if $P_{\text{MC}} \ll 1$ and if the probability \mathcal{P}_+ that a photon entering the line from the blue side will escape to the red side without undergoing any incoherent scattering satisfies $\mathcal{P}_+ \ll 1$.

E. Incorporation in the level code

In principle, modifications to transport in the entire $n^1P^o - 1^1S$ series, the quadrupole series ($n^1D - 1^1S$), and intercombination series ($n^3P^o - 1^1S$) of He I could lead to acceleration of He I recombination. To make the problem computationally tractable, the hierarchy of higher-order n contributions needs to be cut off where there are diminishing returns. The integral solution to the transport equations with complete redistribution (Sec. IV), while not accurate for $n^1P^o - 1^1S$ rates, gives a quick estimate of whether, for example, continuum effects become more and more important for higher n , or die away. We evaluate the probabilities at $z = 1606$, at the end of He I recombination where the continuum effects are expected to be largest, using the integral Eq. (53). It is found that in the intercombination lines, continuum effects become small for $n > 4$ (the ratio of the probabilities with and without continuous opacity approaches 1). For quadrupole transitions ($n^1D - 1^1S$), the corrections are significant out to moderate n (modifying the escape probability by a factor of ~ 2 at $n = 8$). In the $n^1P^o - 1^1S$ series, continuum effects lead to significant modifications to the escape probability (by a factor of ~ 100 at $n = 9$ toward the end of He I recombination)—the entire $n^1P^o - 1^1S$ series sees significant corrections. (One mitigating factor that makes the calculation practical is that only the $2^1P^o - 1^1S$ line dominates recombination rates.) Based on these estimates, we calculate corrections to transport within the line up to $n = 6$ in the $n^1P^o - 1^1S$ series, up to $n = 4$ in the inter-

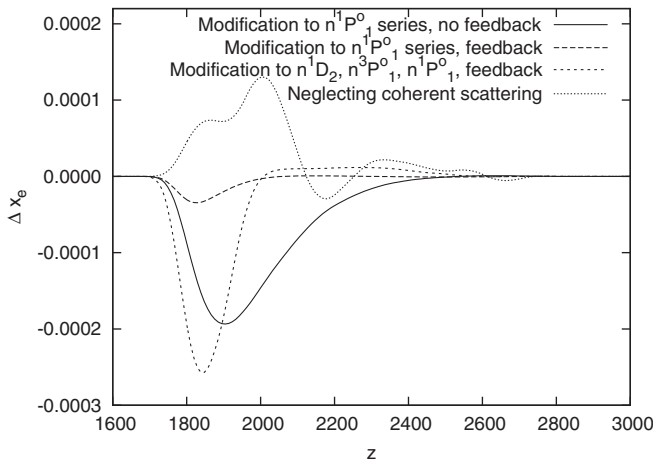


FIG. 10. Modification to the He I recombination history due to continuum opacity in the $n^1D - 1^1S$, $n^3P^o - 1^1S$, and $n^1P^o - 1^1S$ lines (and where coherent scattering through $2^1P^o - 1^1S$ is neglected) relative to a model where only continuum opacity in the $2^1P^o - 1^1S$ line is accounted for. The total effect on x_e is at the level of 10^{-4} . Without feedback, $n^1P^o - 1^1S$ slightly speeds recombination relative to just $2^1P^o - 1^1S$ —the allowed rates from $n > 2$ to the ground state are accelerated. Coherent scattering through $2^1P^o - 1^1S$ is also seen to be negligible for the recombination history.

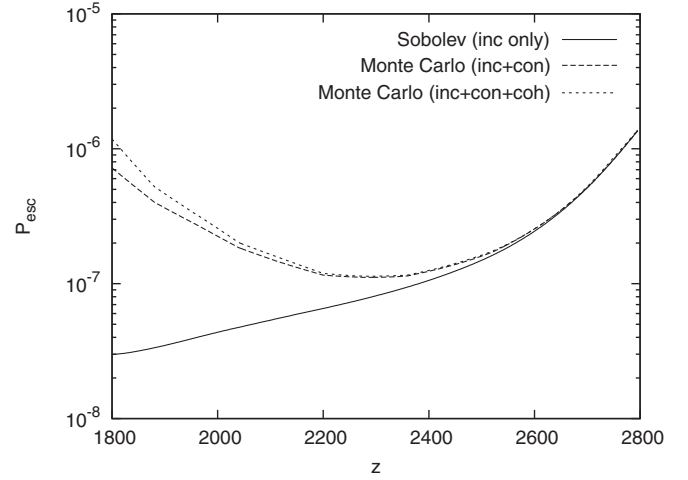


FIG. 11. The modified escape probability from $^4\text{He } 2^1P^o - 1^1S$ during He I recombination, comparing the results of the standard Sobolev approximation and the modification due to continuous opacity with and without coherent scattering. Once coherent scattering is introduced, photon diffusion effects increase the escape probability by increasing the span of frequencies traversed by the scattering photon before it escapes. These probabilities are log-interpolated over the grid of x_{HeI} and z used in the level code. We find that the effect of doubling the grid resolution and with it the smoothness of the interpolated probability is negligible.

combination lines ($n^3P^o - 1^1S$), and $n = 6$ in the quadrupole lines ($n^1D - 1^1S$). The $n^1P^o - 1^1S$ series is treated via the Monte Carlo technique, while the others are treated here using the integral method of Sec. IV. (Figure 10 shows that higher allowed transitions are negligible. In Paper III we will show results where the Monte Carlo method was used for intercombination and quadrupole lines as well.) Figure 11 shows the escape probabilities subject to H I opacity (with and without coherent scattering) for $2^1P^o - 1^1S$ derived from the Monte Carlo method, relative to the ordinary Sobolev results.

Both the Monte Carlo simulation and analytic integral methods of finding the escape probability are prohibitively slow to run in real time with the level code. In the Monte Carlo method, computing the large number of coherent scatters for one photon trajectory in the He I $n^1P^o - 1^1S$ series is very time consuming. In the analytic integral method developed for complete redistribution, the variety of scales in the line profile gives, generally, integrands with large dynamic ranges that need to be known to high accuracies. For this reason, we generate tables of the escape probability over a range of parameters and log-interpolate to find the probabilities in the level code.

The escape probability is a function of the coherent, incoherent, and continuum optical depths, and the matter temperature, which sets the Gaussian width for the line,

$$P_{\text{esc}}(\{\tau_{\text{coh}}, \tau_{\text{inc}}, \eta_c, T_m, \Gamma_{\text{line}}\}). \quad (101)$$

The wing width is set by Γ_{line} . We will project to a more natural parameter space for the level code,

$$\{\tau_{\text{coh}}, \tau_{\text{inc}}, \eta_c, T_m, \Gamma_{\text{line}}\} \rightarrow \left\{ z, \frac{n_{\text{HI}}}{n_{\text{HI,Saha}}}, x_{\text{HeI}} \right\}, \quad (102)$$

since for a given cosmology the latter parameter set determines the former. We calculate tables for 11 linearly spaced z values between 1400 and 3000, inclusive, and 21 logarithmically spaced x_{HeI} values from 2×10^{-5} to 0.08. When we double the fineness of the probability grid over the parameters, the change in free electron density $|\Delta x_e|$ has a maximum of $\sim 5 \times 10^{-4}$ at $z \sim 1900$. The neutral hydrogen population is taken to be the evolution determined by the reference level code. This is very nearly Saha until the end of He I recombination, by which time we find that He I has been relaxed to equilibrium. (That is, whether you assume the H I population is Saha or evolves through in the full recombination treatment should matter little for the evolution of the He I ground state: even before neutral hydrogen departs significantly from equilibrium, He I is already relaxed into equilibrium, by that point.) This set of probabilities required ~ 4 days to evaluate over 50×3.2 GHz computer nodes. The convergence criterion is described in Appendix C, and shown to converge to 1.25% fractional error in probability with negligible bias. Doubling the number of Monte Carlo trials led to a maximum change of $|\Delta x_e| < 10^{-4}$, and resampling with a

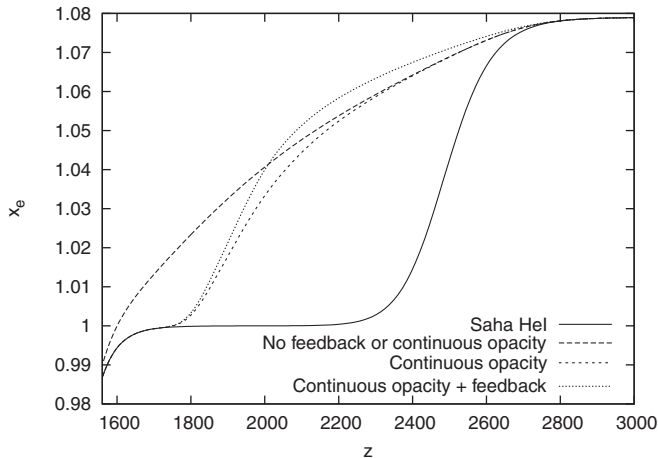


FIG. 12. Modifications to the He I recombination history from the inclusion of feedback and continuum opacity in He I lines, compared to a Saha He I recombination history and the standard He I recombination history. Continuous opacity starts to become important at $z \sim 2100$ (as suggested by Fig. 7), and pushes the He I evolution to a Saha by $z \sim 1800$. The beginning of H I recombination is visible here starting at $z \sim 1700$, and for later times x_e drops precipitously. The modifications to He I recombination suggested here are twofold: at early times during He I recombination, feedback slows recombination, and at later times, continuous opacity accelerates recombination relative to standard models.

different random generator (Numerical Recipes `ran2` instead of `ran3` [67]) gives a change $|\Delta x_e| < 1.5 \times 10^{-4}$. (More convergence tests are described in Paper III.)

The result of including these in the level code is shown in Fig. 12. Here, we can test the diminishing-returns set of modified lines by running a level code with: (1) just $2^1P^o - 1^1S$ modifications, (2) modifications to the $n^1P^o - 1^1S$ series up to $n = 6$, (3) $2^1P^o - 1^1S$ and the 3 intercombination lines, and (4) the $n^1P^o - 1^1S$ series up to $n = 6$, plus the three intercombination lines, shown in Fig. 10. It is apparent that most of the effect is due to modification to the $2^1P^o - 1^1S$ escape probability, leading to relaxation of the “ $n = 2$ ” bottleneck and further that coherent scattering is only a small contribution to the recombination history. This greatly improves prospects for including continuum effects in a practical level code through modifications to $2^1P^o - 1^1S$ under the approximations developed in Sec. IV (without coherent scattering).

VI. CONCLUSION

The efforts of a new generation of precision small-scale CMB temperature anisotropy experiments need to be complemented by confidence that the underlying theory is well understood. Recent results [40–42] have brought up the possibility that new effects may modify the H I and He I recombination histories. Here we have examined and extended several of these recently proposed effects: the matter temperature evolution and the intercombination and quadrupole lines of He I. We also introduce two new effects: feedback of radiation between lines (nonlocal radiative transport), and the effect of continuum opacity from photoionization of neutral hydrogen on transport within and between lines. The effect of feedback between lines, which has previously been neglected is also shown to be a significant effect at the $\sim 1\%$ level by using an iterative method to include the effect. (Paper II and III will treat two-photon processes, electron and ^3He scattering, and rare decays.)

The striking new effect has been the introduction of continuum opacity due to H I photoionization in the He I $2^1P^o - 1^1S$ transition. We presented two methods of understanding this physics, an integral solution to the radiative transport equations for complete redistribution, and a Monte Carlo method for partial redistribution (to include strong coherent scattering effects). This is found to dramatically increase the escape probability and speed up He I recombination once continuum effects in the line become important. These effects, in combination with the inclusion of the intercombination line as suggested by [41], paint a very different picture of He I recombination—one where the recombination accelerates after $z \sim 2200$ leading to very little overlap with the H I recombination. The speed-up is a generic feature of any effects that facilitate the formation of ground state He I, though of course the details depend on the kinetics of the specific mechanism.

Now that the interpretation of many important cosmological parameters depend on slight shifts (such as evidence for inflation from the primordial slope n_s), it will be crucial to understand even subpercent corrections to the recombination history from various slow processes. We have examined several corrections here and more are considered in Paper II and Paper III. Once a set of corrections to hydrogen and helium recombination are solidified, the next step will be to parametrize a set of corrections to a recombination model in a fast, easy-to-use package that can be plugged into CMB calculations and parameter estimations. Distilling the modified escape probabilities for a set of cosmological parameters into a new recombination code will be the subject of later work.

ACKNOWLEDGMENTS

E. S. acknowledges the support from grants from NASA No. LTSAA03-000-0090 and NSF No. PHY-0355328. We acknowledge useful conversations with Jens Chluba, Bruce Draine, Jim Peebles, Doug Scott, Uroš Seljak, and Rashid Sunyaev. We also thank Joanna Dunkley for critical readings and comments prior to publication.

APPENDIX A: ATOMIC LEVELS AND RADIATIVE RATES

1. H I model atom

The full model H I atom has 445 levels up to a maximum principal quantum number $n_{\max} = 400$. The individual l -sublevels are resolved for $n \leq 10$. The energies of each level are determined from the exact nonrelativistic formula $E_{nl} = -R_H/n^2$, where the hydrogen Rydberg constant is $R_H/h = 3.2881$ PHz. The degeneracy factors are $g_{nl} = 2(2l + 1)$ for the l -resolved levels and $g_n = 2n^2$ for the unresolved levels. Throughout, we have used a smaller set of 245 levels, identical to the full model, except truncated at $n_{\max} = 200$. Inclusion of the remaining levels up to $n_{\max} = 400$ will be important for late-stage H I recombination, but negligible for He I recombination.

The bound-bound electric dipole Einstein coefficients between l -resolved levels are determined by integration of the exact wave functions. For cases where the upper sublevel is unresolved ($n_u > 10$), we compute a weighted average of the Einstein coefficient, with the weights determined by the degeneracy factors. This gives the appropriate decay rate in the limit where the sublevels are populated according to their statistical ratios. For transitions with $n_l > 10$ we used the Gaunt factor approximation of Ref. [82], Eq. (1.38), with the correction described in the appendix of Ref. [83]. Direct summation of the Einstein coefficients shows that this yields an error of 1.2% for the worst case ($n_l = 11$, $n_u - n_l = 1$). We have not included the H I electric quadrupole lines ($1s - nd$, $n \geq 3$) because they are at the same frequency as the Lyman lines $1s - np$

and hence do not yield acceleration of the H I recombination process. (This is not the case for He I.)

The bound-free cross sections for $n \leq 10$ are obtained from TOPbase [84]; for $n > 10$, the l -sublevels are unresolved and we have used the Gaunt factor approximation.

The H I atom possesses a metastable $2s$ level, which decays by emission of two electric dipole photons. We have used the two-photon frequency distribution and the spontaneous lifetime estimate $\Lambda_{\text{HI}} = 8.2249 \text{ s}^{-1}$ from Ref. [85].

2. He I model atom

The He I model atom has 289 levels up to a maximum principal quantum number $n_{\max} = 100$. For all values of n we resolve singlet (“para-He I”) versus triplet (“ortho-He I”) levels. The l -sublevels are resolved for $n \leq 10$. We include only configurations of the form $1s nl$ as the doubly excited configurations are all unbound. The energy levels for the l -resolved levels in He I are taken from the NIST Atomic Spectral Database, based on Ref. [86], except for $n = 9, 10$, $l > 6$, for which hydrogenic values were used. For the $n > 10$ levels in which the value of l is unresolved, we have used the Rydberg formula (which produces as accurate a value as can be considered meaningful given that the various l levels are not strictly degenerate). The degeneracy factors are $g_{nLS} = (2L + 1)(2S + 1)$ for L -resolved levels and $g_{nS} = n^2(2S + 1)$ for unresolved levels. Note that in ortho-He I, there are multiple allowed values of J for given L and S , which correspond to fine structure levels; we do not resolve these.

For the allowed bound-bound transition rates, we combined data for several sources. For transitions between two l -resolved levels, the electric dipole oscillator strengths for allowed $S - P^o$ and $P^o - D$ transitions were obtained from Ref. [87] for upper levels with $n \leq 9$. The $1^1S - 10^1P^o$ transition rate is from Ref. [88] and other $S - P$ and $P - D$ rates with upper level $n = 10$ are from TOPbase [84]. For $D - F^o$, $F^o - G$, etc. transitions, we used the hydrogenic rates since the $l \geq 2$ states are well approximated as an electron orbiting a pointlike He^+ ion. For transitions between an l -resolved lower level and an unresolved upper level ($n > 10$), we first compute the fully l -resolved Einstein coefficients and then average. These l -resolved rates are taken as hydrogenic for $P - D$, $D - F$, etc. transitions. For $1^1S - n^1P^o$ transitions ($n < 10$), we use the asymptotic formula of Ref. [89]. (This formula is only 1.4% different from TOPbase at $n = 10$.) The Coulomb approximation [90] is used for all other $S - P^o$ transitions. For transitions between two unresolved levels ($n_l > 10$), we have used the hydrogenic Gaunt factor approximation.

In He I recombination, the intercombination and forbidden lines can be competitive with allowed lines as a mechanism of decay to the ground state because the al-

lowed lines become very optically thick. In particular we consider the series of intercombination lines He I] $1^1S - n^3P^o$ ($n \geq 2$) and forbidden lines [He I] $1^1S - n^1D$ ($n \geq 2$). For the He I] $1^1S_0 - n^3P_1^o$ lines with $n = 2, 3$ we have used the Einstein coefficients estimated by Ref. [91]; these are extrapolated as $A \propto n^{-3}$ for larger n . (Note that the Einstein coefficients are usually quoted for the fine structure-resolved $n^3P_1^o$ level. Since our code does not resolve the fine structure these coefficients must be divided by 3 since only 3 of the $9n^3P^o$ states have $J = 1$.) For the [He I] $1^1S - n^1D$ lines with $3 \leq n \leq 6$, we have used the oscillator strengths calculated by Ref. [92]. For $n > 6$ the oscillator strengths have been extrapolated with the asymptotic expansion $f \propto n^{-3}$.

Like H I, the He I atom possesses a metastable singlet state 2^1S_0 that decays by emission of two electric dipole photons. The two-photon rate used here is $\Lambda_{\text{HeI}} = 50.94 \text{ s}^{-1}$, as determined by Ref. [93]. The two-photon spectrum of He I was determined by the following formula, which was fitted to the results of Ref. [93]:

$$\phi(\nu) = \frac{19.602}{\nu_{1^1S_0-2^1S_0}} \frac{\zeta^3(1.742 - 7.2\zeta + 12.8\zeta^2)}{(\zeta + 0.03)^2}, \quad (\text{A1})$$

where $\nu_{1^1S_0-2^1S_0} = 4.9849 \text{ PHz}$ is the frequency difference between the ground and metastable states, and $\zeta = \nu(\nu_{1^1S_0-2^1S_0} - \nu)/\nu_{1^1S_0-2^1S_0}^2$ is between 0 and 1/4.

3. He II model ion

The He II ion has one electron and hence in nonrelativistic theory all rates can be obtained by scaling of H I. The energy levels are rescaled in proportion to $Z^2\mu$, where Z is the atomic number and μ is the reduced mass. The ratio of these factors for He II versus H I is 4.001 787. The bound-bound rate coefficients scale as $(Z^2\mu)^2$ and the photoionization cross sections scale as $(Z^2\mu)^{-1}$. The two-photon decay rate Λ scales as $(Z^2\mu)^3$. The He II model atom is l -resolved up to $n = 10$ and has a maximum principal quantum number $n_{\text{max}} = 100$, for a total of 145 levels.

APPENDIX B: INTEGRATION OF THE TRANSPORT EQUATION FOR COMPLETE REDISTRIBUTION AND CONTINUOUS OPACITY

In this appendix we discuss how the transport equation with continuous opacity is integrated to find the continuum absorption probability, Eq. (53). Rybicki and Hummer [72] develop a convenient analytic approximation to the transport solution in the case of a Gaussian profile with high optical depth. This gives good intuition for the combinations of factors that contribute to the escape probability. For example, it suggests that if the escape probability for a line i is known, then an approximate scaling (in their limits) can be used to find the escape probability from j ,

$$P_{\text{esc},j} \sim \left(\frac{P_{\text{esc},i}\tau_{\text{inc},i}}{\sigma_{\text{D},i}\eta_{\text{C},i}} \right) \frac{\sigma_{\text{D},j}\eta_{\text{C},j}}{\tau_{\text{inc},j}}. \quad (\text{B1})$$

There are three reasons why we would like a more general solution. First, the high optical depth limit is not applicable to intercombination or quadrupole lines during recombination, though they have nearly Gaussian profiles. Second, it is desirable to be able to use the macroscopic transport equations as a cross-check for the photon Monte Carlo methods developed in the next section for the $n^1P^o - 1^1S$ series, before the effect of coherent scattering is ‘‘turned on.’’ This requires solving Eq. (53) with the Voigt profile. (It also shows directly why complete redistribution is a dangerous assumption in the $n^1P^o - 1^1S$ series.) Third, He I recombination rates are sensitive to the probabilities set by Eq. (53), so a high-precision numerical result is necessary. These constraints are met by directly integrating Eq. (53) with the Voigt profile.

The Voigt profile presents two characteristic frequency scales: slowly varying functions in wings, and rapidly varying functions in the core. In the Doppler core, we can follow an analysis similar to [72] and note that in the inner integrand,

$$\exp\left\{-\tau_{\text{inc}} \int_{\nu}^{\tilde{\nu}} \phi(y) dy\right\}, \quad (\text{B2})$$

the contribution is small unless the integral in the exponent is less than τ_{inc}^{-1} . Yet, for the small differences between ν and $\tilde{\nu}$, the integrand is nearly linear,

$$\int_{\nu}^{\tilde{\nu}} \phi(\nu') d\nu' \approx \phi(\nu)(\tilde{\nu} - \nu). \quad (\text{B3})$$

Thus, in the Doppler core, the integral depends on evaluations of the integral over the Voigt profile on very small scales. The Voigt function and its integral are time consuming to evaluate. Further, a linear interpolation lookup table must have sufficient resolution in the core, and breadth in the wings for Eq. (53) to be evaluated accurately. We use the Gubner’s series [94] in the core region and switch to a fourth order asymptotic expansion of the Voigt profile in the wings. (In the boundary between the two regimes, we estimate the error in the asymptotic expansion by using the next higher order and ensure that differences between the two approaches are negligible.) The Voigt function and its integral are tabulated out to 10 000 Doppler widths with 50 values per Doppler width, exploiting the symmetry of the profile and its integral. These are interpolated using a cubic spline and Eq. (53) is integrated using a 61-point Gauss-Kronrod adaptive integration scheme. (This is necessary because the integrand of Eq. (53) carries its support over a widely varying range of $\tilde{\nu}$.) To apply the numerical results of this integral to the recombination setting, P_{C} is precalculated for a range of τ_{inc} and $\eta_{\text{C}}\Delta\nu_{\text{D}}$, and then log-interpolated.

APPENDIX C: MONTE CARLO METHOD: IMPLEMENTATION

Monte Carlo radiative transfer methods have been used extensively in the literature [75–81]. We follow an approach similar to Hirata [75], and use an algorithm to draw atomic velocity distributions that is discussed clearly in Lee [95,96]. A general atomic scattering process can be represented by the joint probability function of a photon with ν_{in} scattering against the atom coherently to produce a photon of ν_{out} through the scattering angle χ , $P(\nu_{\text{out}}, \chi | \nu_{\text{in}})$.

In coherent scattering, the photon is emitted with the same frequency it was absorbed in the atom’s rest frame, and its emission direction relative to the incoming photon is drawn from the angular distribution associated with the transition. The Doppler shift formula gives an expression for the frequency shift between incoming and outgoing photons in the lab frame,

$$\Delta\nu = (f_{\parallel} + \alpha)(1 - \cos\chi) - f_{\perp} \sin\chi, \quad (\text{C1})$$

where $\mathbf{f} = \nu_0 \mathbf{v}/c$, for the transition frequency ν_0 , and $\alpha = h\nu_0^2/(m_p c^2)$. Throughout, \parallel labels the component of a vector in the direction from which the photon came, and \perp labels the component perpendicular to this direction and in the plane of scattering. Thus, the change in frequency between the input and output states in the lab frame is uniquely specified through χ , f_{\parallel} , and f_{\perp} . These three quantities are stochastic, where f_{\parallel} and f_{\perp} depend on the thermodynamics of the gas, and χ is determined by the quantum mechanical scattering distribution. The distribution of the angle χ between outgoing states and incoming states for dipole scattering is given by (over the range $0 \leq \chi \leq \pi$) [75],

$$P(\chi)d\chi = \frac{3}{8}(1 + \cos^2\chi) \sin\chi d\chi. \quad (\text{C2})$$

We can scale the atomic velocity relative to the other velocity scale in the problem, the characteristic thermal velocity, $u = v\sqrt{m/(2k_B T)}$. This gives the convenient expression $f_{\parallel} = (\Delta\nu_D)u_{\parallel} = \sqrt{2}\sigma_D u_{\parallel}$, where $\Delta\nu_D$ is the Doppler width in standard notation, and σ_D^2 is the variance of the Doppler Gaussian. In the perpendicular direction, the distribution of atomic velocities is thermal, $\propto e^{-u_{\perp}^2}$. Bayes’ rule gives the distribution of u_{\parallel} based on known distributions as

$$\begin{aligned} P(u_{\parallel}|x_{\text{in}}) &= \frac{P(x_{\text{in}}|u_{\parallel})P(u_{\parallel})}{P(x_{\text{in}})} \\ &= \frac{a}{\pi H(a, x_{\text{in}})} \frac{e^{-u_{\parallel}^2}}{a^2 + (x_{\text{in}} - u_{\parallel})^2}. \end{aligned} \quad (\text{C3})$$

Here $H(a, x)$ is the Voigt profile,

$$H(a, x) = \frac{a}{\pi} \int_{-\infty}^{\infty} \frac{e^{-y^2} dy}{a^2 + (x - y)^2}, \quad (\text{C4})$$

$x = (\nu - \nu_0)/\Delta\nu_D$, and a is the Voigt width parameter:

$$a = \frac{\Gamma_{\text{line}}}{4\pi\Delta\nu_D}. \quad (\text{C5})$$

Typically $a \ll 1$, indicating that the Lorentzian width of the line is very small compared to the Doppler width. Lee [95,96] presents a rejection method to randomly draw from this distribution.

When a photon is emitted by an incoherent process—i.e. it reaches an excited level u either by a radiative transition from another excited level, or by recombination—the outgoing photon has no knowledge of the phase space distribution of preexisting line photons, so the probability distribution function for an outgoing photon is just the Voigt profile. Because the Voigt profile is the convolution of the Doppler Gaussian distribution and the Cauchy distribution, a Voigt-distributed random number is easily implemented as the sum of random numbers drawn from each distribution.

The distance between scatters for small frequency shifts is given by $\ell \approx cH^{-1}(z)\nu_0^{-1}\Delta\nu$ (for some central frequency ν_0 and shift $\Delta\nu$). Over the travel times associated with the escape of one photon, the universe has expanded very little, and the line depth parameters are effectively constant.

In standard Sobolev theory, where the fate of the photon is either that it escapes or is absorbed in an incoherent process, it is clear what is meant by an escape probability. The transport problem for He I with continuum opacity is not as clear-cut. Coherent, incoherent, continuum, and redshift processes are all active, so there are several choices about what “escape” and “scatter” mean. As shown in the main text however, there is one specific number we need to know: given a photon was just emitted in the line through an incoherent process, what is the probability P_{MC} that it will escape through redshifting or continuum absorption before it is absorbed in an incoherent process? The easiest way to measure P_{MC} with the Monte Carlo simulation is to inject many photons whose initial frequency distribution is the Voigt profile, and follow them until they escape (i.e. redshift out of the line or get absorbed by H I) or are reabsorbed in an incoherent process. Here the range of frequencies simulated is ± 360 THz with a bin size of 0.36 GHz. (Using a smaller span or less resolution leads to escape probabilities that are biased high at early times during He I recombination, because absorption can occur far in the wings at early times when the incoherent depth is high and the continuum depth is small. Doubling the boundary and halving the frequency step size does not improve the results, within these tolerances.) The basic steps in the Monte Carlo simulation are:

- (1) Draw a photon from the Voigt distribution, representing emission from an incoherent process.
- (2) Draw the optical depth that the photon traverses

before scattering from the exponential distribution, $P(\delta\tau)d(\delta\tau) = e^{-\delta\tau}d(\delta\tau)$. The next frequency where the photon scatters is given implicitly by

$$\begin{aligned}\tilde{\tau} &= \int_{\nu_{\text{start}}}^{\nu} \left[(\tau_{\text{inc}} + \tau_{\text{coh}})\phi(\tilde{\nu}) + \frac{d\tau}{d\nu}(\tilde{\nu}) \right] d\tilde{\nu} \\ &\equiv \int_{\nu_{\text{start}}}^{\nu} d\tilde{\nu}\eta(\tilde{\nu}),\end{aligned}\quad (\text{C6})$$

where we have identified the integrand $d\tau_{\text{tot}}/d\nu$ as $I(\nu)$. This is implemented numerically by choosing frequency bins ($\Delta\nu = 0.36$ GHz) and determining whether a photon crosses that bin, or is absorbed. If the bins are chosen to be small enough, then the integrand is nearly linear over the bin,

$$\eta(\nu)|_i = \frac{\eta_{i+1} - \eta_i}{\Delta\nu} + \eta_i. \quad (\text{C7})$$

Integrating this gives a quadratic expression for the fraction x of the bin that the photon traversed:

$$\frac{\eta_{i+1} - \eta_i}{2\eta_i}x^2 + x = \frac{\delta\tau}{(\Delta\nu)\eta_i}. \quad (\text{C8})$$

This can either be solved quadratically, or by working to first order in small bins. We will use the latter approach for small bins,

$$x_0 = \frac{\delta\tau}{(\Delta\nu)\eta_i} \quad \text{and} \quad x = x_0 \left(1 - x_0 \frac{\eta_{i+1} - \eta_i}{2\eta_i} \right). \quad (\text{C9})$$

The fraction of the bin traversed indicates whether the photon scattered in the bin, or leaves. If it escaped the bin, then we move the photon to the start of the next bin and go to step 2. If it traversed less than the whole bin, we find the frequency in the bin where it scatters ν_{scatter} , and go to step 3.

- (3) Draw a uniform random number between zero and $\frac{d\tau_{\text{tot}}}{d\nu}(\tilde{\nu}_{\text{scatter}})$ and determine the type of event (incoherent scatter/absorption, coherent scatter, or H I continuum absorption).
- (4) If the photon coherently scatters, draw the scattered atom's velocity and angle between incoming and outgoing states and use Eq. (C1) to find the photon energy after scattering, and go to step 2. If the photon is incoherently scattered by He I, undergoes photoelectric absorption by H I, or redshifts through a predefined simulation boundary, start a new photon in step 1.

The Monte Carlo procedure leaves one issue open, namely, the convergence criterion. We repeat the Monte Carlo simulation until 6400 photons escape from the line, which should enable P_{MC} to be determined to a fractional error of $6400^{-1/2} = 0.0125$. A possible concern with this procedure (or any other in which the number of photons simulated is not fixed before running the

Monte Carlo simulation) is that the result could be biased if the convergence criterion depends on the results of the simulation. We addressed this question by replacing the function that decides whether the photon escapes with a random number generator that returns escape a known fraction P_{MC} of the time and ‘‘no escape’’ (incoherent scatter) a fraction $1 - P_{\text{MC}}$ of the time. This produces a very fast code that allows us to map the distribution of the estimated escape probability \hat{P}_{MC} as a function of the true P_{MC} . Across the relevant range of P_{MC} (down to 10^{-6}) we find that \hat{P}_{MC} has a bias $\langle \hat{P}_{\text{MC}} \rangle / P_{\text{MC}} - 1$ whose absolute value is $< 0.1\%$, and a standard deviation $\sigma(\hat{P}_{\text{MC}}) / P_{\text{MC}} \approx 0.0125$.

APPENDIX D: RELATION OF ESCAPE PROBABILITY METHODS

In this appendix, we consider the relation of the Monte Carlo method to the analytic solution of Sec. IV and to the usual Sobolev escape method. We show explicitly that the solution to the transport equations considered here reduce to those of Sec. IV if $f_{\text{coh}} \rightarrow 0$. We then proceed to investigate the conditions under which the Monte Carlo solution is equivalent to the Sobolev escape method.

1. Relation to case of no coherent scattering

Here we connect the formalism developed in Secs. V B and V C to the analysis of Sec. IV, which neglected coherent scattering.

The transport equation for line processes and the continuum, ignoring the coherent scattering diffusion term gives

$$\frac{\partial \mathcal{N}}{\partial \nu} = \eta_c[\mathcal{N}(\nu) - \mathcal{N}_C] + \tau_{\text{inc}}\phi(\nu)[\mathcal{N}(\nu) - \mathcal{N}_L^{(0)}]. \quad (\text{D1})$$

This can be solved for $\bar{\mathcal{N}}$ analogously to the derivation in Sec. IV,

$$\bar{\mathcal{N}} = \mathcal{N}_L^{(0)} + P_{\text{esc}}^{(\text{IV})}(\mathcal{N}_C - \mathcal{N}_L^{(0)}), \quad (\text{D2})$$

where $P_{\text{esc}}^{(\text{IV})} \equiv P_S - \Delta\bar{I}_L$ is the escape probability derived in Sec. IV (cf. Eq. (55)). Comparing this to the analysis of Sec. V C, in particular, Eq. (76) we find the correspondence

$$\bar{\xi} = 1 - P_{\text{esc}}^{(\text{IV})}. \quad (\text{D3})$$

Plugging into the transport result, Eq. (89), one finds that P_{esc} (which modulates the rate) is now

$$P_{\text{esc}} = \frac{P_{\text{esc}}^{(\text{IV})}f_{\text{inc}}}{1 - f_{\text{coh}}P_{\text{esc}}^{(\text{IV})}}. \quad (\text{D4})$$

This reduces to $P_{\text{esc}} = P_{\text{esc}}^{(\text{IV})}$ in the limit that scattering in the line is purely incoherent, as expected.

2. Relation of the Monte Carlo and Sobolev methods

Next we consider the relation between this escape probability and the traditional Sobolev probability P_S used in recombination codes in the *absence* of coherent scattering. The Sobolev escape calculation in its usual form assumes complete redistribution over the steady-state line profile and neglects continuum opacity [73,97]. Complete redistribution is an accurate assumption in pure-resonance rate problems where the radiation field is forced into equilibrium with the line over most of its central frequency extent by the high incoherent scattering rate (typically when the wing is optically thick to incoherent scattering). Also it is trivially valid if the scattering optical depth is dominated by incoherent scattering. Diffusion from Doppler shifts in repeated coherent scattering events has been studied extensively through its redistribution function, the Fokker-Planck approximation (accurate away from the Doppler core), and Monte Carlo methods [73,75,95,97]. This diffusion tends to broaden the jump in the radiation phase space density distribution on the blue side of the line, but does not significantly suppress (or enhance) \mathcal{N} near line center or modify the atomic transitions rates. Thus, for practical purposes in a recombination level code with pure resonant line processes and no continuous opacity, there is very little loss in assuming complete redistribution and steady-state radiation fields.

During recombination, there are two general categories of lines connecting to the ground state to consider: (1) $f_{\text{inc}} \approx 1$ so that $\tau_{\text{inc}} \approx \tau_S$ (intercombination and forbidden lines) or (2) f_{inc} is small but τ_{inc} is large, i.e. $\tau_{\text{coh}} \gg \tau_{\text{inc}} \gg 1$ (allowed lines such as $n^1P^o - 1^1S$ in He I or the Lyman series in H I). We consider what happens in each type of line with continuum opacity off ($\eta_c = 0$).

For case (1), $f_{\text{coh}} \ll 1$ but $f_{\text{inc}} \approx 1$; then it is immediate that $P_{\text{esc}} \approx P_S$. The treatment of case (2) is more complicated. We begin by integrating Eq. (78) over frequency with $\eta_c = 0$ to get

$$\begin{aligned} \xi_+ - \xi_- &= \tau_{\text{coh}} \left[\int \phi(\nu) \xi(\nu) d\nu \right. \\ &\quad \left. - \iint \phi(\nu') \xi(\nu') p(\nu|\nu') d\nu' d\nu \right] \\ &\quad + \tau_{\text{inc}} \int \phi(\nu) [\xi(\nu) - 1] d\nu. \end{aligned} \quad (\text{D5})$$

Here ξ_{\pm} is the value of ξ on the blue (+) or red (-) side of the line. The term multiplying τ_{coh} vanishes since the redistribution probability p integrates to unity. Also $\xi_+ = 0$ because of boundary conditions. The last term simplifies to $\tau_{\text{inc}}(1 - \bar{\xi})$ or $\tau_{\text{inc}} P_{\text{MC}}$. If we turn off continuum opacity ($\eta_c = 0$), this then simplifies to

$$P_{\text{MC}} = \frac{\xi_-}{\tau_{\text{inc}}}, \quad (\text{D6})$$

which is much less than 1. Then from Eq. (100):

$$P_{\text{esc}} \approx \frac{(\xi_-/\tau_{\text{inc}})f_{\text{inc}}}{1 - f_{\text{coh}}P_{\text{MC}}} \approx \frac{\xi_- f_{\text{inc}}}{\tau_{\text{inc}}} = \frac{\xi_-}{\tau_S}. \quad (\text{D7})$$

In order to proceed we must understand the behavior of ξ_- in the case with no continuum opacity. This can be done by considering a thought experiment in which we inject photons into the Monte Carlo simulation on the far blue side of the line instead of using the Voigt profile. In this modified Monte Carlo simulation, the photon probability distribution Π^{mod} satisfies

$$\begin{aligned} \frac{\partial \Pi^{\text{mod}}}{\partial \nu} &= \tau_{\text{inc}} \phi(\nu) \Pi^{\text{mod}}(\nu) + \tau_{\text{coh}} \left[\phi(\nu) \Pi^{\text{mod}}(\nu) \right. \\ &\quad \left. - \int \phi(\nu') \Pi^{\text{mod}}(\nu') p(\nu|\nu') d\nu' \right], \end{aligned} \quad (\text{D8})$$

with the boundary condition $\Pi^{\text{mod}}(\nu) = \Gamma_{\text{inj}}/H\nu_{ul}$ in the blue wing since in the absence of the line photons redshift at a rate $\dot{\nu} = -H\nu_{ul}$. Defining the quantity

$$X(\nu) = 1 - \frac{H\nu_{ul}}{\Gamma_{\text{inj}}} \Pi^{\text{mod}}(\nu), \quad (\text{D9})$$

we see that $X(+\infty) = 0$ and that $X(\nu)$ satisfies

$$\begin{aligned} \frac{d}{d\nu} X(\nu) &= \tau_{\text{coh}} \left[\phi(\nu) X(\nu) - \int \phi(\nu') X(\nu') p(\nu|\nu') d\nu' \right] \\ &\quad + \tau_{\text{inc}} \phi(\nu) [X(\nu) - 1], \end{aligned} \quad (\text{D10})$$

where we have used the symmetry relation $\int \phi(\nu') p(\nu|\nu') d\nu' = \phi(\nu)$ to eliminate the terms that come from the 1 term in Eq. (D9). Now $X(\nu)$ satisfies the same integro-differential equation as $\xi(\nu)$ in Eq. (78), and has the same boundary condition $X(+\infty) = 0$. Therefore we have $X(\nu) = \xi(\nu)$ and $\xi_- = X_-$. This means that the photon frequency distribution on the red side of the line is

$$\Pi_-^{\text{mod}} = \frac{\Gamma_{\text{inj}}}{H\nu_{ul}} (1 - \xi_-). \quad (\text{D11})$$

Therefore on the red side of the line, the frequency distribution of the photons is suppressed by a factor of $1 - \xi_-$. Therefore, in the absence of continuum opacity, the probability P_{trans} that a photon injected on the blue side of the line manages to redshift through the line without any incoherent scattering/absorption is $1 - \xi_-$. Conversely, $\xi_- = 1 - P_{\text{trans}}$ is the probability that such a photon is incoherently scattered/absorbed in the line. This provides a simple physical interpretation of ξ_- .

In the case where the line is very optically thick into the damping wings, we expect the line transmission probability $P_{\text{trans}} \ll 1$ and hence $\xi_- \approx 1$. It follows that $P_{\text{esc}} \approx \tau_S^{-1}$. This is in agreement with the Sobolev value for $\tau_S \gg 1$. Thus, in both of the limiting cases (1) and (2) where the continuum opacity is small, P_{esc} is well approximated by P_S . The approximation $P_{\text{esc}} \approx P_S$ can fail if the coherent depth is very large, while the incoherent depth is optically thin. This could occur at very early times during recomb-

nation in the $n^1P^o - 1^1S$ series, for example. Yet, for $2^1P^o - 1^1S$, the difference between $f_{\text{inc}}P_{\text{inc}}$ and P_S is $<10^{-4}$ (likewise for the $n^1P^o - 1^1S$ series considered here). The distinction is thus negligible in the overall recombination history.

APPENDIX E: PHOTONS IN THE HE I CONTINUUM

Recombination to the ground state is usually ignored because the photon that is generated immediately reionizes another bound atom. This is a single-species picture. When bound-free rates in helium and hydrogen interact, the recombination photons that would have ionized He I can instead be absorbed by H I. This accelerates He I recombination by allowing recombinations directly to 1^1S . (It also forces hydrogen slightly out of equilibrium.) The direct 1^1S recombination rate in He I should roughly scale as the recombination rate to 1^1S_0 times the probability that the ionizing photon is absorbed by hydrogen instead of by He I. In this appendix, we develop this effect in more detail and show that it can be neglected.

It is tedious to solve the full transport problem for $\mathcal{N}(\nu)$ subject to bound-free processes in He I and H I, and then integrate to find the photoionization and recombination rates. We will instead track the total number of photons with energies above 24.6 eV (from recombination to He I), and develop a method to calculate an effective cross section and photoionization rate for both He I and H I by photons from region. Recombination rates can be calculated through detailed balancing of the photoionization rate.

A similar mechanism is active in He II, and in principle one should also consider simulating the possibility of direct recombination to H I 1s. In H I, there is no coupling between species and the answer is straightforward. In He II, recombination proceeds too close to equilibrium for this effect to matter.

We lump the radiation field into frequency regions for photons above threshold for each species and consider the loss of photons in a given lumped region due to bound-free processes, and redshift. Note that the integral of the radiation phase space density over a region is not enough to entirely specify the behavior. The number of photons that redshift out of the region depends on the phase space density at its red boundary. Because the spectrum is blackbody dominated, we will approximate the radiation phase space density at the boundary by its blackbody value there.

If the perturbations to the radiation field caused by bound-free processes are over frequency scales which are large compared to the exponential fall-off of the blackbody radiation field and the radiation field is close to equilibrium, then an effective constant cross section (near threshold) in each lumped frequency region provides a good first approximation.

Define the number of photons per hydrogen nucleon above the ionization threshold of species s as

$$X_{\text{th},s}^> = \int_{E_{\text{th},s}}^{\infty} \frac{n_\gamma(E)}{n_H} dE = \frac{h^3}{n_H} \int_{\nu_{\text{th},s}}^{\infty} \mathcal{N}(\nu) \left(\frac{8\pi\nu^2}{c^3} \right) d\nu. \quad (\text{E1})$$

(Throughout, we will use the subscript s to denote the species. Unless stated otherwise in this appendix, all occupation variables, photoionization cross sections, and photoionization or recombination rates are taken from the ground state of that species.) To a good approximation, at these energies stimulated recombinations can be neglected because the photons are from well into the tail of the blackbody distribution. One can then write the photoionization rate from the ground state due to these photons as

$$\beta_s \approx \sigma_{\text{eff},s} \frac{X_{\text{th},s}^> c n_H}{h^3}, \quad (\text{E2})$$

where $\sigma_{\text{eff},s}$ is an effective cross section. By the principle of detailed balance the recombination rate directly to the ground state is

$$\alpha_s \equiv \sigma_{\text{eff},s} \left(\frac{n_s}{n_e n_c} \right)^{\text{LTE}} \frac{X_{\text{th},s}^> \text{bb} c n_H}{h^3}. \quad (\text{E3})$$

The effective cross sections are determined by equating Eq. (E2) to Eq. (4) for a thermal distribution of photons $\mathcal{N} = e^{-h\nu/k_B T}$, i.e.

$$\begin{aligned} \sigma_{\text{eff},s} &= \frac{8\pi c^{-2} \int_{\nu_{\text{min}}}^{\infty} \nu^2 \sigma(\nu) e^{-h\nu/k_B T} d\nu}{X_{\text{th},s}^>} \\ &\approx \sigma(\nu_{\text{min}}) + \frac{k_B T}{h} \sigma'(\nu_{\text{min}}), \end{aligned} \quad (\text{E4})$$

where σ' denotes the derivative of the cross section with respect to frequency. Note that this assumes the distribution of radiation above the threshold ν_{min} is distributed as $\mathcal{N} \propto e^{-h\nu/k_B T}$. This is obviously true in equilibrium if $h\nu \gg k_B T$ but may be violated in the real universe. Physically we do not expect large deviations from this proportionality if the main source of opacity is photoionization, because the photons above ionization threshold should develop a phase space distribution $\mathcal{N} = e^{-(h\nu - \mu_\gamma)/k_B T}$, where the photon chemical potential μ_γ is determined by the non-Saha behavior of the ionization stages, e.g.

$$\mu_\gamma = \mu_{\text{HII}} + \mu_e - \mu_{\text{HI}} = k_B T \ln \frac{n_e n_{\text{HII}} / n_{\text{HI}}}{(n_e n_{\text{HII}} / n_{\text{HI}})_{\text{Saha}}}, \quad (\text{E5})$$

if the source of opacity is H I. This may not happen if the photon sees opacity from two competing species (e.g. H I and He I) whose relative deviations from Saha equilibrium are different. The most severe case would occur if the cross sections vary rapidly with frequency such that e.g. H I opacity dominates at some frequencies and He I at others. However the H I and He I cross sections are smooth functions of frequency in the regime of interest (i.e. far

below the He I double-excitation resonance region), so we expect that the current “one group” approach is adequate for assessing whether continuum photons are important.

Then, the total bound-free rate to the ground state is

$$\frac{dx_s}{dt} = \frac{cn_H}{h^3} \sigma_{\text{eff},s} \left[n_e x_c \left(\frac{n_s}{n_e n_c} \right)^{\text{LTE}} X_{\text{th},s}^{>,bb} - x_s X_{\text{th},s}^{>} \right]. \quad (\text{E6})$$

In this picture, in addition to the state occupations evolving, the lumped radiation fields $X_{\text{th},s}^{>}$ evolve, and can be included as additional “states” in the level code. The total number of photons in a frequency region is not conserved. Thus the evolution equations must account for photons that redshift out of the region, as well as those that are injected or removed by bound-free processes. Taking the derivative gives a loss rate from the region,

$$\frac{dX_{\text{th},s}^{>}}{dt} = \frac{1}{n_H} \frac{d(X_{\text{th},s}^{>} n_H)}{dt} + 3HX_{\text{th},s}^{>} = \frac{8\pi}{c^3} \frac{h^3 H}{n_H} \nu_{\text{th}}^3 \mathcal{N}(\nu_{\text{th}}). \quad (\text{E7})$$

Here ν_{th} is the ionization threshold frequency of the species. Assuming an $\mathcal{N} \propto e^{-h\nu/k_B T}$ spectrum, the rate of redshifting of photons is (under the considerations developed for He I recombination),

$$\frac{1}{X_{\text{th},s}^{>}} \frac{dX_{\text{th},s}^{>}}{dt} \Big|_{bb} = \left(\frac{h\nu}{k_B T_r} \right)^3 \left[\frac{h\nu}{k_B T_r} \left(\frac{h\nu}{k_B T_r} + 2 \right) + 2 \right]^{-1} H.$$

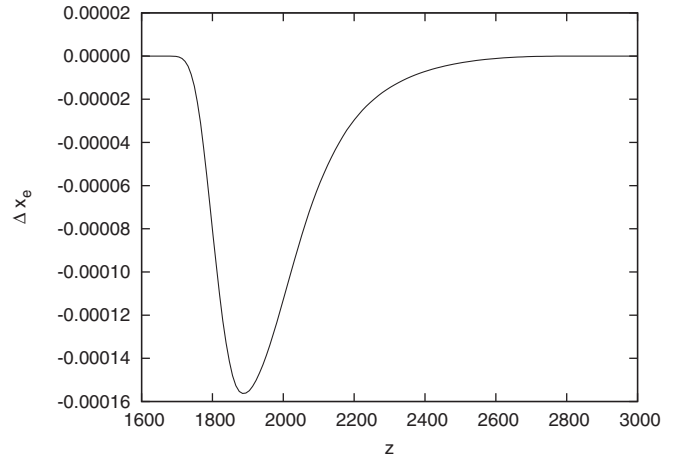


FIG. 13. Recombination directly to He I 1^1S can occur because He I recombination photons can ionize neutral hydrogen, before they ionize He I. This would tend to accelerate recombination. Here we show that this effect leads to a maximum fractional deficit of electrons of around 10^{-4} .

With this choice of variables and tracked states, we can accommodate the interaction between He I and H I bound-free rates—the overall effect on the free electron occupation fraction is shown in Fig. 13.

-
- [1] D.N. Spergel, R. Bean, O. Doré, M.R. Nolta, C.L. Bennett, J. Dunkley, G. Hinshaw, N. Jarosik, E. Komatsu, L. Page *et al.*, *Astrophys. J. Suppl. Ser.* **170**, 377 (2007).
- [2] M. Tegmark, M. A. Strauss, M. R. Blanton, K. Abazajian, S. Dodelson, H. Sandvik, X. Wang, D.H. Weinberg, I. Zehavi, N.A. Bahcall *et al.*, *Phys. Rev. D* **69**, 103501 (2004).
- [3] A. E. Lange, P. A. Ade, J. J. Bock, J. R. Bond, J. Borrill, A. Boscaleri, K. Coble, B. P. Crill, P. de Bernardis, P. Farese *et al.*, *Phys. Rev. D* **63**, 042001 (2001).
- [4] A. H. Jaffe, P. A. Ade, A. Balbi, J. J. Bock, J. R. Bond, J. Borrill, A. Boscaleri, K. Coble, B. P. Crill, P. de Bernardis *et al.*, *Phys. Rev. Lett.* **86**, 3475 (2001).
- [5] C. Pryke, N. W. Halverson, E. M. Leitch, J. Kovac, J. E. Carlstrom, W. L. Holzzapfel, and M. Dragovan, *Astrophys. J.* **568**, 46 (2002).
- [6] M. E. Abroe, A. Balbi, J. Borrill, E. F. Bunn, S. Hanany, P. G. Ferreira, A. H. Jaffe, A. T. Lee, K. A. Olive, B. Rabii *et al.*, *Mon. Not. R. Astron. Soc.* **334**, 11 (2002).
- [7] J. A. Tauber, *Adv. Space Res.* **34**, 491 (2004).
- [8] A. Kosowsky, *New Astron. Rev.* **47**, 939 (2003).
- [9] J. Ruhl, P. A. R. Ade, J. E. Carlstrom, H.-M. Cho, T. Crawford, M. Dobbs, C. H. Greer, N. w. Halverson, W. L. Holzzapfel, T. M. Lanting *et al.*, in *Astronomical Structures and Mechanisms Technology*, edited by J. Antebi and D. Lemke, SPIE Proceedings Vol. 5495 (SPIE-International Society for Optical Engineering, Bellingham, WA, 2004); in *Millimeter and Submillimeter Detectors for Astronomy II*, edited by J. Zmuidzinas, W. S. Holland, and S. Withington, SPIE Proceedings Vol. 5498 (SPIE-International Society for Optical Engineering, Bellingham, WA, 2004), p. 11.
- [10] C. L. Kuo, P. A. R. Ade, J. J. Bock, C. Cantalupo, M. D. Daub, J. Goldstein, W. L. Holzzapfel, A. E. Lange, M. Lueker, and M. Newcomb *et al.*, *Astrophys. J.* **600**, 32 (2004).
- [11] R. Stompor, M. Abroe, P. Ade, A. Balbi, D. Barbosa, J. Bock, J. Borrill, A. Boscaleri, P. de Bernardis, P. G. Ferreira *et al.*, *Astrophys. J. Lett.* **561**, L7 (2001).
- [12] C. B. Netterfield, P. A. R. Ade, J. J. Bock, J. R. Bond, J. Borrill, A. Boscaleri, K. Coble, C. R. Contaldi, B. P. Crill, P. de Bernardis *et al.*, *Astrophys. J.* **571**, 604 (2002).
- [13] N. W. Halverson, E. M. Leitch, C. Pryke, J. Kovac, J. E. Carlstrom, W. L. Holzzapfel, M. Dragovan, J. K. Cartwright, B. S. Mason, S. Padin *et al.*, *Astrophys. J.* **568**, 38 (2002).
- [14] T. J. Pearson, B. S. Mason, A. C. S. Readhead, M. C. Shepherd, J. L. Sievers, P. S. Udomprasert, J. K. Cartwright, A. J. Farmer, S. Padin, S. T. Myers *et al.*, *Astrophys. J.* **591**, 556 (2003).
- [15] K. Grainge, W. F. Grainger, M. E. Jones, R. Kneissl, G. G.

- Pooley, and R. Saunders, *Mon. Not. R. Astron. Soc.* **329**, 890 (2002).
- [16] R. Génova-Santos, J. A. Rubiño-Martín, R. Rebolo, K. Cleary, R. D. Davies, R. J. Davis, C. Dickinson, N. Falcón, K. Grainge, C. M. Gutiérrez *et al.*, *Mon. Not. R. Astron. Soc.* **363**, 79 (2005).
- [17] M. White, *Astrophys. J.* **555**, 88 (2001).
- [18] S. Dodelson, W. H. Kinney, and E. W. Kolb, *Phys. Rev. D* **56**, 3207 (1997).
- [19] H. V. Peiris, E. Komatsu, L. Verde, D. N. Spergel, C. L. Bennett, M. Halpern, G. Hinshaw, N. Jarosik, A. Kogut, M. Limon *et al.*, *Astrophys. J. Suppl. Ser.* **148**, 213 (2003).
- [20] R. A. Sunyaev and Y. B. Zeldovich, *Astrophys. Space Sci.* **7**, 3 (1970).
- [21] P. J. E. Peebles and J. T. Yu, *Astrophys. J.* **162**, 815 (1970).
- [22] J. R. Bond and G. Efstathiou, *Mon. Not. R. Astron. Soc.* **226**, 655 (1987).
- [23] W. Hu, N. Sugiyama, and J. Silk, *Nature (London)* **386**, 37 (1997).
- [24] J. Silk, *Astrophys. J.* **151**, 459 (1968).
- [25] W. Hu and M. White, *Astrophys. J.* **479**, 568 (1997).
- [26] A. Lewis, J. Weller, and R. Battye, *Mon. Not. R. Astron. Soc.* **373**, 561 (2006).
- [27] S. Seager, D. D. Sasselov, and D. Scott, *Astrophys. J. Suppl. Ser.* **128**, 407 (2000).
- [28] P. J. E. Peebles, *Astrophys. J.* **153**, 1 (1968).
- [29] Y. B. Zeldovich, V. G. Kurt, and R. A. Sunyaev, *Zh. Eksp. Teor. Fiz.* **55**, 278 (1968).
- [30] T. Matsuda, H. Satō, and H. Takeda, *Prog. Theor. Phys.* **42**, 219 (1969).
- [31] T. Matsuda, H. Sato, and H. Takeda, *Prog. Theor. Phys.* **46**, 416 (1971).
- [32] I. E. Liubarskii and R. A. Sunyaev, *Astron. Astrophys.* **123**, 171 (1983).
- [33] S. Lepp and J. M. Shull, *Astrophys. J.* **280**, 465 (1984).
- [34] H. J. Fahr and R. Loch, *Astron. Astrophys.* **246**, 1 (1991).
- [35] D. Galli and F. Palla, *Astron. Astrophys.* **335**, 403 (1998).
- [36] S. Seager, D. D. Sasselov, and D. Scott, *Astrophys. J. Lett.* **523**, L1 (1999).
- [37] R. A. Sunyaev and J. Chluba, arXiv:0710.2879.
- [38] W. Y. Wong, A. Moss, and D. Scott, arXiv:0711.1357.
- [39] J. Chluba and R. A. Sunyaev, *Astron. Astrophys.* **478**, L27 (2008).
- [40] J. Chluba and R. A. Sunyaev, *Astron. Astrophys.* **446**, 39 (2006).
- [41] V. K. Dubrovich and S. I. Grachev, *Astron. Lett.* **31**, 359 (2005).
- [42] P. K. Leung, C. W. Chan, and M.-C. Chu, *Mon. Not. R. Astron. Soc.* **349**, 632 (2004).
- [43] W. Y. Wong and D. Scott, *Mon. Not. R. Astron. Soc.* **375**, 1441 (2007).
- [44] E. E. Kholupenko and A. V. Ivanchik, *Astron. Lett.* **32**, 795 (2006).
- [45] W. Y. Wong and D. Scott, arXiv:astro-ph/0612322 [Astrophysics (Engl. Transl.) (to be published)].
- [46] A. Lewis, *Phys. Rev. D* **76**, 063001 (2007).
- [47] V. K. Dubrovich, *Astron. Lett.* **33**, 645 (2007).
- [48] J. Chluba and R. A. Sunyaev, *Astron. Astrophys.* **475**, 109 (2007).
- [49] J. Chluba and R. A. Sunyaev, arXiv:0705.3033.
- [50] E. E. Kholupenko, A. V. Ivanchik, and D. A. Varshalovich, *Mon. Not. R. Astron. Soc.* **378**, L39 (2007).
- [51] S. I. Grachev and V. K. Dubrovich, arXiv:0801.3347.
- [52] J. Chluba, J. A. Rubiño-Martín, and R. A. Sunyaev, *Mon. Not. R. Astron. Soc.* **374**, 1310 (2007).
- [53] W. Hu, D. Scott, N. Sugiyama, and M. White, *Phys. Rev. D* **52**, 5498 (1995).
- [54] R. Gopal and S. K. Sethi, *Mon. Not. R. Astron. Soc.* **363**, 521 (2005).
- [55] R. A. Battye, R. Crittenden, and J. Weller, *Phys. Rev. D* **63**, 043505 (2001).
- [56] M. Mapelli and A. Ferrara, *Mon. Not. R. Astron. Soc.* **364**, 2 (2005).
- [57] N. Padmanabhan and D. P. Finkbeiner, *Phys. Rev. D* **72**, 023508 (2005).
- [58] P. J. E. Peebles, S. Seager, and W. Hu, *Astrophys. J. Lett.* **539**, L1 (2000).
- [59] M. Mapelli, A. Ferrara, and E. Pierpaoli, *Mon. Not. R. Astron. Soc.* **369**, 1719 (2006).
- [60] S. Hannestad, *New Astron. Rev.* **6**, 17 (2001).
- [61] E. Pierpaoli, *Phys. Rev. Lett.* **92**, 031301 (2004).
- [62] P. P. Avelino, C. J. A. P. Martins, G. Rocha, and P. Viana, *Phys. Rev. D* **62**, 123508 (2000).
- [63] S. A. Bonometto and X. Shouping, *Astron. Astrophys.* **157**, L7 (1986).
- [64] G. B. Rybicki and A. P. Lightman, *Radiative Processes in Astrophysics*, edited by G. B. Rybicki and A. P. Lightman (Wiley-VCH, New York, 1986), , p. 400.
- [65] R. S. Sutherland, *Mon. Not. R. Astron. Soc.* **300**, 321 (1998).
- [66] X. Chen and J. Miralda-Escudé, *Astrophys. J.* **602**, 1 (2004).
- [67] W. H. Press, S. A. Teukolsky, W. T. Vetterling, and B. P. Flannery, *Numerical Recipes In C. The Art of Scientific Computing* (Cambridge University Press, Cambridge, England, 1992), 2nd ed.
- [68] E. R. Switzer and C. M. Hirata, *Phys. Rev. D* **72**, 083002 (2005).
- [69] J. G. Baker and D. H. Menzel, *Astrophys. J.* **88**, 52 (1938).
- [70] J. H. Krolik, *Astrophys. J.* **338**, 594 (1989).
- [71] J. H. Krolik, *Astrophys. J.* **353**, 21 (1990).
- [72] D. G. Hummer and G. B. Rybicki, *Astrophys. J.* **293**, 258 (1985).
- [73] D. G. Hummer and G. B. Rybicki, *Astrophys. J.* **387**, 248 (1992).
- [74] D. G. Hummer, *Mon. Not. R. Astron. Soc.* **125**, 21 (1962).
- [75] C. M. Hirata, *Mon. Not. R. Astron. Soc.* **367**, 259 (2006).
- [76] Z. Zheng and J. Miralda-Escudé, *Astrophys. J.* **578**, 33 (2002).
- [77] J. R. M. Bonilha, R. Ferch, E. E. Salpeter, G. Slater, and P. D. Noerdlinger, *Astrophys. J.* **233**, 649 (1979).
- [78] C. Bernes, *Astron. Astrophys.* **73**, 67 (1979).
- [79] L. J. Caroff, P. D. Noerdlinger, and J. D. Scargle, *Astrophys. J.* **176**, 439 (1972).
- [80] L. H. Auer, *Astrophys. J.* **153**, 783 (1968).
- [81] L. W. Avery and L. L. House, *Astrophys. J.* **152**, 493 (1968).
- [82] D. H. Menzel and C. L. Pekeris, *Mon. Not. R. Astron. Soc.* **96**, 77 (1935).
- [83] A. Burgess, *Mon. Not. R. Astron. Soc.* **118**, 477 (1958).
- [84] W. Cunto, C. Mendoza, F. Ochsenbein, and C. J. Zeppen, *Astron. Astrophys.* **275**, L5 (1993).

- [85] H. Nussbaumer and W. Schmutz, *Astron. Astrophys.* **138**, 495 (1984).
- [86] W. C. Martin, *Phys. Rev. A* **36**, 3575 (1987).
- [87] A. Kono and S. Hattori, *Phys. Rev. A* **29**, 2981 (1984).
- [88] F. Khan, G. S. Khandelwal, and J. W. Wilson, *Astrophys. J.* **329**, 493 (1988).
- [89] G. S. Khandelwal, F. Khan, and J. W. Wilson, *Astrophys. J.* **336**, 504 (1989).
- [90] D. R. Bates and A. Damgaard, *Phil. Trans. R. Soc. A* **242**, 101 (1949).
- [91] C. Laughlin, *J. Phys. B* **11**, L391 (1978).
- [92] N. M. Cann and A. J. Thakkar, *J. Phys. B* **35**, 421 (2002).
- [93] G. W. F. Drake, *Phys. Rev. A* **34**, 2871 (1986).
- [94] J. A. Gubner, *J. Phys. A* **27**, L745 (1994).
- [95] J.-S. Lee, *Astrophys. J.* **218**, 857 (1977).
- [96] J. S. Lee, *Astrophys. J.* **255**, 303 (1982).
- [97] G. B. Rybicki and I. P. dell'Antonio, *Astrophys. J.* **427**, 603 (1994).